The Dissertation Committee for Pietro Scaduto Certifies that this is the approved version of the following dissertation:

Synaptic Excitatory to Inhibitory imbalance in Alzheimer's Disease

Committee:

Agenor Limon, Ph.D., Mentor and Chair

Giulio Taglialatela, Ph.D.

Balaji Krishnan, Ph.D.

Owen Hamill, Ph.D.

Mingshan Xue, Ph.D.

Giulio Taglialatela, Ph.D, Dean ad Interim, Graduate School

Synaptic Excitatory to Inhibitory imbalance in Alzheimer's Disease

by

Pietro Scaduto, MS, Ph.D.

Dissertation

Presented to the Faculty of

The University of Texas Medical Branch

in Partial Fulfillment

of the Requirements

for the Degree of

Doctor of Philosophy

The University of Texas Medical Branch

September 2021

Dedication

To Enzo, Maria, and Federica.

My permanent center of gravity.

Acknowledgements

I would like to thank my mentor, Dr. Limon, for teaching me the light and dark sides of the independency, "*Try not. Do or do not, there is no try*".

Thanks to the Italian family in Galveston for being a second family.

Thanks to my family for understanding and always support my choices.

Synaptic Excitatory to Inhibitory imbalance in Alzheimer's Disease

Publication No._____

Pietro Scaduto, MS, Ph.D.

The University of Texas Medical Branch, 2021

Supervisor: Agenor Limon, Ph.D.

Alzheimer's disease is the most common cause of dementia worldwide, and it is characterized by progressive impairment of cognitive performance, brain atrophy, neuronal and synaptic loss, and abnormal aggregation of amyloid beta and tau proteins. Notably, prodromal Alzheimer's disease is characterized by mild cognitive impairment, increments in the occurrence of seizures and abnormal electroencephalographic activity. Clinical and animal model studies suggest that hyperexcitability and cognitive impairment may be mechanistically linked, through synaptic abnormalities that disturb the excitatory/inhibitory balance (E/I ratio) in circuits vulnerable to Alzheimer's disease pathology. We measured electrophysiological, anatomical, transcriptional, and cellular E/I ratios in human brain. Our findings establish a strong correlational link between E/I imbalance and loss of cognition; and showed a pro-excitatory shift of this balance in brain regions known to be hyperactive in Alzheimer's disease subjects.

TABLE OF CONTENTS

List of Tables

List of Figures

List of Illustrations

List of

Abbreviations

AD: Alzheimer's disease
AMPA: α-amino-3-hydroxy-5-methyl-4-isoxazolepropionic acid
APOE: apolipoprotein ε
APP- β: amyloid β precursor protein
ATP: adenosine tri-phosphate
Aβ: amyloid β
Aβ-42: amyloid β Protein Fragment 1-42
CN: cognitive normal
CNS: central nervous system
ConA: concanavalin A
CSF: cerebral spinal fluid
CTZ: cyclothiazide
DCF: dichlorofluorescein
DCFH-DA: dichlorofluorescein diacetate
*DLG*4: PSD-95 gene
DMN: default mode network
DS: down Syndrome
E/I ratio: global synaptic Excitatory to inhibitory ratio
EC50: half of the apparent affinity
ELISA: enzyme-linked immunosorbent assay
fAD: familial Alzheimer's disease
FDT: fluorescence deconvolution tomography
GABA: gamma aminobutyric acid
$GABA_AR$s: gamma aminobutyric acid receptor type A.
GFAP: glial fibrillary acid protein
GPHN: gephyrin gene / mRNA
GPHN: gephyrin protein
Hipp: hippocampus
IFN: interferon
IFN-β-1a: interferon-β1a
IGluR: glutamate inotropic receptors
IL: interleukin
Ir: immunoreactivity
MCI: mild cognitive impairment
MDA: malondialdehyde
MRI: magnetic resonance imaging
MS: multiple sclerosis
MSM: microtransplantation of synaptic membranes
MTS: ([3-(4,5-dimethylthiazol-2-yl)-5-(3-carboxymethoxyphenyl)-2-(4-sulphophenyl)-2H-tetrazolium]
NF-kB: transcription factor nuclear factor-kB
NMDA: N-methyl-D-aspartate
PCx: parietal cortex
PET: positron emission tomography
PiB: Pittsburgh Compound B
PLSD: Fisher's Protected Least Significant Difference
PMI: *post-mortem* interval
PNF-kB: phosphorylated NF-kB
PS1: presenilin-1
PS2: presenilin-2
PSD-95: postsynaptic density protein 95
ptau: phosphorylated tau
ROS: reactive oxygen species
SAD: sporadic Alzheimer's disease
SSAD: staging of severity of AD
Syn: synaptophysin
RI%: recognition index
TBA: thiobarbituric acid
TCx: Temporal cortex
TEVC: two electrode voltage clamp
TGF-β1: Transforming growth factor-beta1
TNF-α: tumor necrosis factor
τ: time constant
ρ: non-parametric Spearman's

CHAPTER 1. INTRODUCTION

ALZHEIMER'S DISEASE

Alzheimer's disease (AD) is an age-related neurodegenerative disease characterized by progressive impairment of cognitive performance, brain atrophy, and neuronal lesions as plaques and tangles (Illustration 1 [1,2] and 2[1]) . Neuronal lesions are composed by abnormal accumulations of proteins prone to misfold such as amyloid-β (Aβ)

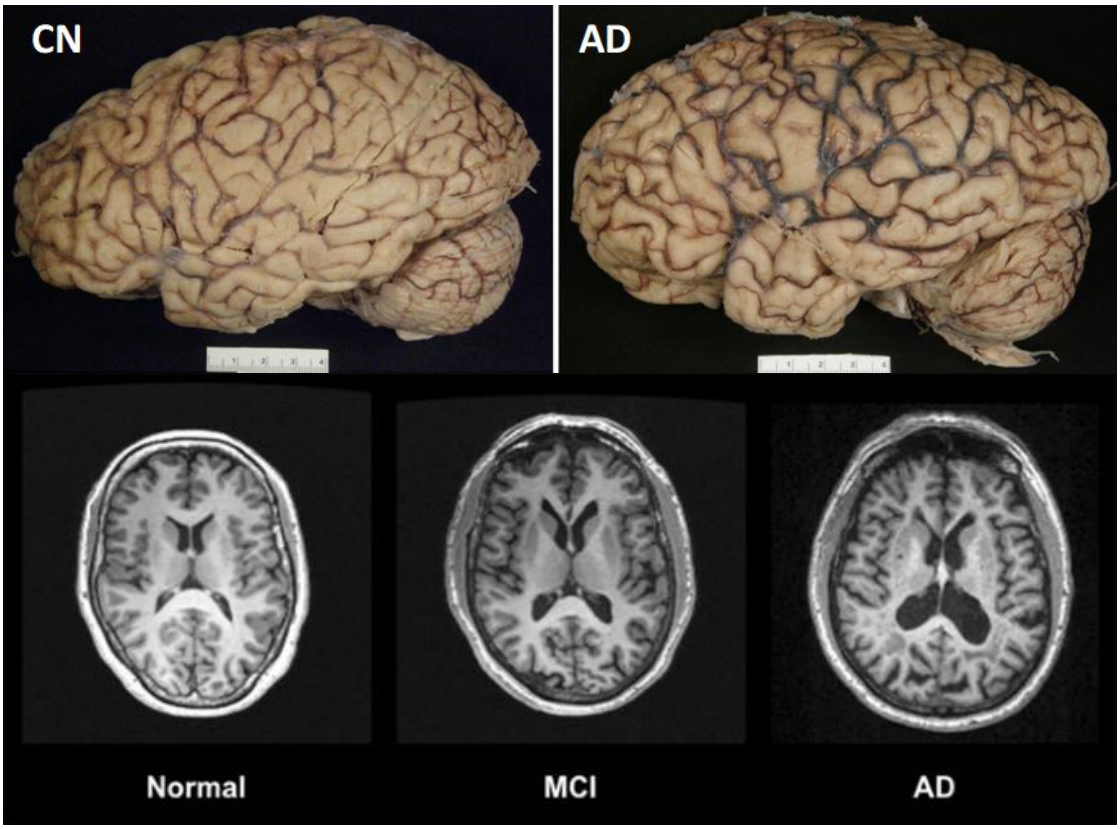

Illustration 1. **Top left,** lateral view of a cognitively normal (CN) brain and **Top right,** an AD brain. **Bottom,** magnetic resonance imaging scan. Horizontal section from a CN, mild cognitive impaired (MCI) and AD subjects. Modified figures with permission from [1,2]

and tau proteins[3]. Aβ is a small peptide (39–43 amino acids) involved in neuronal survival and in synaptic excitability [4,5]. Tau is a microtubule-associated protein that stabilize microtubules in neurons [6,7]. Both, Aβ and Tau play physiological roles at the synapse, but

under pathologic conditions, they form aggregates in response to degeneration of specific types of neurons [8,9].

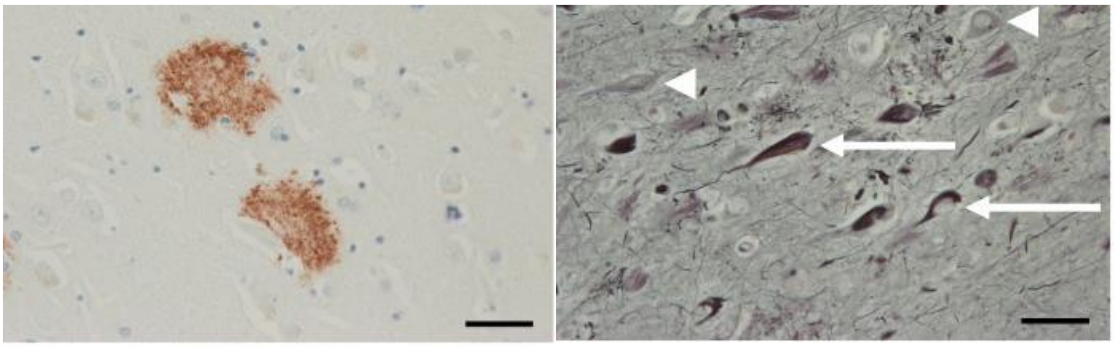

Illustration 2. Alzheimer Senile Plaques and Neurofibrillary Tangles. Left. Immunohistochemistry of affected AD 's tissue using antibodies directed against Aβ peptides demonstrates the presence of senile plaques. Right. Silver staining of neurofibrillary tangles develop from intracellular pre-tangles containing misfolded tau (mature tangles = arrows; pre-tangles = arrowheads). Modified figure with permission from [1]

AD is the most common cause of dementia worldwide, only in U.S there are 6 millions of people affected, and its incidence is projected to increase 3-fold over the next 30 years [10]. In 2020, the cost of healthcare for AD treatment is estimated at $305 billion, and today there is no disease-modifying treatment available [10]. The only approved drugs (Donepezil, Rivastigmine, Galantamine, Memantine) by the U.S. Food and Drug Administration (FDA) provide limited symptomatic relief targeting neurons excitability[11]. Recently in 2021, a new drug targeting plaques aggregation (aducanumab) has been approved with some controversy because it failed to prove efficacy in one of the major clinical trials [12].

HISTORY OF ALZHEIMER'S DISEASE

AD was first described in the early 1900's by Dr. Aloysius Alzheimer and collaborators [13], by reporting the first clinical case of a "paranoid with progressive sleep and memory disturbance, aggression, and confusion symptoms". After several decades, in 1984, a task force group composed of leading experts intended to establish and describe a clinical criteria for the diagnosis of AD [14]. AD was thus defined as a brain disorder characterized by progressive dementia. Its pathologic characteristics are degeneration of neurons; presence of neuritic plaques, characterized by Aβ aggregates surrounded by a

dense network of nerve cell processes; and intracellular neurofibrillary tangles that are product of the misfolding and aggregation of tau protein (Illustration 2, [15]). Moreover, AD was defined as a clinical-pathologic entity, which is diagnosed definitely at autopsy and in life as possible or probable AD [14]. Over the last three decades, researchers have worked to improve the AD diagnosis accuracy in living people, trying to avoid errors derived from misinterpreting prototypical clinical syndromes without neuropathological verification. The clinical diagnosis of potential AD is established by testing cognitive function as memory, problem solving, attention, counting, and language; or by measuring Aβ and tau accumulation in cerebrospinal fluid (CSF); or by molecular imaging as positron emission tomography (PET)-amyloid and –tau assays and structural magnetic resonance imaging (MRI) in the brain [16,17].

In 1991, Heiko and Eva Braak studied 83 brains from non-demented and demented individuals. Histological sections from these brains were examined for extracellular amyloid deposits and intraneuronal neurofibrillary changes to develop the first classification of AD brain region and severity progression, also known as Braak staging [18]. This classification is still widely accepted to evaluate the severity of the disease on post-mortem brain, and it is mainly based on neurofibrillary tangles distribution. The pathology is divided in 6 stages: the first two stages (transentorhinal phase) were characterized by mild or severe transentorhinal alteration, the 3rd and 4th stages (limbic phase) were defined by the spread of the neurodegeneration in the proper entorhinal cortex, and the 5th and 6th stages (isocortical phase) were marked by destruction of many cortical association areas [18]. A neuropathologic diagnosis of AD is possible using a semiquantitative estimation of neuritic plaque density as recommended by the Consortium to Establish a Registry for Alzheimer's Disease (CERAD)[19,20]; minimum CERAD plaque score is 0 (no neuritic plaques) and maximum score is 3 (frequent plaques).

Despite the considerable progress over the years, the mechanisms behind the neurodegeneration in AD are still not fully understood; and AD lacks convincing disease-modifying therapies.

CLASSIFICATION AND RISK FACTORS

AD can be classified as familial (fAD) or sporadic (sAD), depending on the pathogenesis. The incidence of fAD is lower than 5% and is associated to mutations in three different genes: presenilin-1 (*PS1*), presenilin-2 (*PS2*), and amyloid precursor protein (*APP*) [21,22]. All known fAD mutations are related to the biological cascade controlling either the biosynthesis or the processing of APP [23–25]. Down syndrome, characterized by an extra copy of chromosome 21 in which the APP gene is located, is another genetic risk factor contributing to AD pathogenesis [26]. Sporadic AD (>95%) has a multifactorial onset and the main risk factor is aging with the prevalence of AD rising exponentially after 65 years of age [27]. AD incidence doubles every 5 years after 65 years of age, and even if AD is not always the outcome of aging, after 85 years of age, one in every three subjects is diagnosed with AD [28]. There are other risk factors for AD: lower education, female sex, head trauma, heart disease, smoking, diabetes type 2 and the presence of either 1 or 2 copies of the ε4 allele of the gene for apolipoprotein E (*APOE*) [29]. ApoE is a protein involved in lipid metabolism and consisting in 3 known isoforms: ApoE2, 3 and 4. ApoE3 is the most common variant, ApoE4 seems to contribute to an increased risk for AD and ApoE2 has been shown to be protective. Also physical activity and Mediterranean diet seems to have a protective role as well. [30,31].

Despite the effort to characterize distinct pathological stages, AD pathology is considered as a *continuum*. After a preclinical asymptomatic phase, the first signs of cognitive impairment appear and then there is a progressive worsening of symptoms. Subjects with genetic risks of AD, or showing positive AD biomarkers without fAD mutations in the early stage of the disease, present a cognitive performance below the expected range. These subjects, which are diagnosed with mild cognitive impairment (MCI) [32], are considered to be at an intermediate clinical stage between cognitively intact and AD type dementia [33,34]. Clinical and research studies most commonly test cognitive functioning of AD subjects using the Mini-Mental State Examination (MMSE) or the Cognitive Abilities Screening Instrument (CASI). MMSE is a 20 questions test scored out of 30 points used to measure: orientation, short-term memory, attention, language, and comprehension. CASI is an extended version of MMSE that uses 40 questions and is scored

out of 100 points. Recent studies, allow us to compare cognitive scores from different tests through co-calibration using item response theory (IRT)[35].

HYPERACTIVITY AND SYNAPTIC IMBALANCE IN ALZHEIMER'S DISEASE

Neural excitability depends largely on the synaptic activity [36], and AD is considered a disease of the synapses [37]. Contrary to past reports [37], not only excitatory (glutamatergic) signaling is disrupted in AD, but also inhibitory (gamma aminobutyric acid or GABAergic) signaling [38,39]. The vast majority of synapses in the human brain use glutamate or GABA as neurotransmitters, and together with their own synaptic receptors, these neurotransmitters are critical for slow neurotransmission via metabotropic receptors, and fast neurotransmission via ionotropic receptors. In this study, I will focus on the fast-synaptic transmission.

Glutamate inotropic receptors (iGluRs) are the major mediators of the fast-excitatory synaptic transmission in the mammalian brain. They are transmembrane ligand-gated ion channels composed by a combination of four subunits. IGluRs, based on their subunit composition and pharmacology, these receptors have different physiological properties, and are divided in 3 subclasses: α-amino-3-hydroxy-5-methyl-4-isoxazolepropionic acid receptors (AMPARs), kainate receptors, and N-Methyl-D-aspartic acid receptors (NMDARs). All of them are permeable to cations. Importantly, AMPARs and NMDARs are known to bind Aβ oligomers, which opens these receptors [40].

$GABA_A$ receptors ($GABA_ARs$) are the major mediators of the fast-inhibitory synaptic transmission in the mammalian brain. They are pentameric transmembrane receptors forming a central pore permeable to chloride ions. $GABA_ARs$ are made by the arrangement of five of the nineteen possible subunits, giving to this receptor a large variability of isoforms [41]. Moreover, Aβ oligomers reduce inhibitory post-synaptic currents in neurons via $GABA_AR$ [42].

Glutamatergic and GABAergic synaptic transmissions are constantly tuned to each other during the neurogenesis, adulthood and senescence of the individual[43,44]. This

complex process is named excitation to inhibition balance. It can be defined as the average amount of depolarizing to hyperpolarizing neuronal synaptic currents (global synaptic E/I ratio or just E/I ratio) in a particular region [45]. A balanced E/I ratio is critical for coherent neural coding [46] and its impairment has been associated with the onset of disorders such as schizophrenia, autism and AD [47,48]. Animal models of AD and epilepsy show brain hyperexcitability due to E/I imbalance [49,50], possibly as a result of alteration of glutamatergic and GABAergic neurotransmission [51,52]. Tau seems to be essential in this process since its reduction significantly decreased seizure sensitivity in an animal model of AD [53]. Furthermore, evidence reviewed by Demuro, A [54] shows that Aβ oligomers increase calcium permeability in neurons and glia that could lead to disruption of brain circuits, hyperexcitability and increase of cytokines production [55–57].

Recent evidence suggests that early cognitive alterations are detectable years before meeting criteria for MCI and may allow to predict the progression to dementia. The study of asymptomatic fAD subjects is critical to elucidate the early impairment of AD.

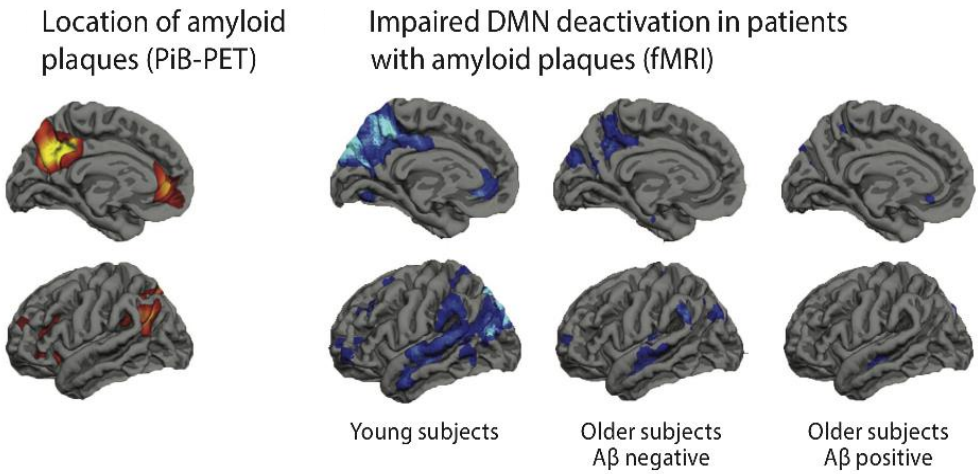

Illustration 3. Deactivation of the default mode network (DMN) is reduced with aging and Aβ burden.. On the left, Anatomic distribution of Aβ burden (yellow and red) detected using Pittsburgh Compound B (PiB) and positron emission tomography (PET). On the right, demonstrating significant task-related decreases in fMRI activity (deactivation shown in blue) during successful encoding of face-name. Modified figure with permission from [68]

Asymptomatic fAD subjects have shown accumulation of tau and Aβ-42 (considered the most toxic isoform of Aβ) in CSF and in the brain parenchyma [58,59], and impairment of

synaptic excitability [60,61] producing hyperactivity of the cerebral cortex years before the onset of clinical AD.

Aberrant excitability has been reported in pre-clinical AD, MCI and AD suggesting that synaptic alterations precede cognitive symptoms and persist over time. Functional MRI analysis revealed that pre-clinical AD in APOE ε4 positive subjects shows temporal and parietal cortex (PCx) hyperactivity during cognitive challenge tasks. The hyperactivation correlated with the degree of decline in memory among subjects who were retested two years later [61]. Also, pre-clinical AD, carrying fully-penetrant genetic alterations in *PS1*, have shown hyperactivation of hippocampus [60]. MCI patients present fMRI hyperactivation in hippocampus during memory task performing, and interestingly, it negatively correlates with temporal and parietal thickness [62]. Reducing the hyperexcitability in MCI patients using an atypical anti-epileptic improved their cognition [34,63]. Subjects with full-blown AD have 6- to 10-fold increase risk of seizures [64], and show similar medial temporal hyperactivity described before (reviewed in [65]). In AD subjects, medial temporal hyperactivity correlates with parietal degeneration, and dysconnectivity between medial temporal lobe and parietal cortices [66].

Interestingly, brain areas in which Aβ start to accumulate are also hyperactive in AD. These areas are functionally interconnected and form a functional network named: *default mode network (*DMN*)* [67–69]. The structural core region of the DMN are the posterior medial and parietal cerebral cortices as well as distinct temporal and frontal modules [70]. The DMN is active at a resting state but needs to be deactivated when the subject is required to perform a task that involve directing attention to an external stimulus [71]. The efficient deactivation of this brain network is critical for attention, memory and language processing [72–74]. Emerging evidence using PET-scan has shown that in AD subjects the accumulation of β-amyloid starts in areas of the DMN causing impairment of the connectivity and deactivation failure (Illustration 3)[68,75]. The DMN is currently considered as a primary locus of AD pathology [76].

AIM OF THE DISSERTATION

Clinical studies and experiments with animal models suggest that synaptic loss may disturb the excitatory to inhibitory balance (E/I ratio) in circuits vulnerable to AD pathology [52,77,78], which in turn could lead to the cortical hyperexcitability that is associated with cognitive impairment [52,79,80]. However, electrophysiological evidence from animal model studies indicates that the activity and strength of excitatory and inhibitory synapses in the cerebral cortex are highly correlated across different cortical activity patterns [46,81]. Thus, synaptic currents, through AMPARs and $GABA_A$Rs, are tightly regulated to preserve the global synaptic E/I ratio within a range that allows for normal network level operations [46,81,82]. Previous work of Limon et *al.,* showed the activity of functional $GABA_A$Rs, both synaptic and extrasynaptic combined, is significantly reduced in the temporal cortex (TCx) of the AD brain, and that this reduction is equal to or greater than the reduction in AMPARs [83]. However, those experiments did not distinguish between synaptic and extrasynaptic $GABA_A$Rs, and thus do not directly address potential changes in the strength of fast inhibitory synaptic currents. Moreover, gene expression for the $GABA_A$R subunit *GABRG2* was more affected than that of *GRIA2* [83], a result that raises the possibility of AD related shifts in the operating characteristics of synaptic receptors. In all, the issue of whether AD differentially affects inhibitory vs. excitatory synapses, and thus E/I balance in cortex, had yet to be resolved. Such information is critical for refining hypotheses about the origins of AD related pathogenesis and pathophysiology, and for development of effective therapies.

Individuals at early stage of AD show MCI, increments in the occurrence of seizures and abnormal electroencephalographic (EEG) activity [52,79,84–87]. As mentioned before, the E/I ratio in principal neurons is maintained at a near constant level by tight homeostatic mechanisms, despite fluctuating activity [88]. Small changes of this ratio can have large effects on neuronal activity that control spike timing, network rhythms and implement functional brain states [46,49,89–93] and since Aβ and tau oligomers production is activity-dependent, hyperexcitability likely accelerates transition to dementia [94,95]. Equally

important, it is not known whether global synaptic E/I imbalance correlate with the severity of cognitive impairment in AD.

The central hypothesis of this dissertation is that brain areas known to be affected by hyperactivity in AD subjects are characterized by an E/I imbalance at the synaptic level. First, we studied the E/I ratio in the PCx of early-onset AD subjects. Then, we evaluated the E/I ratio in brain regions early affected by AD neuropathology (hippocampus and TCx) in MCI and AD. The central hypothesis was addressed via the completion of the specific aims contained within the two scientific manuscripts described below:

Manuscript 1: Increased functional Excitatory to Inhibitory synaptic ratio in parietal cortex of Alzheimer's disease subjects

- Determine the anatomical synaptic E/I ratio by using fluorescence deconvolution tomography (FDT)
- Determine the electrophysiological E/I balance (*e*E/I) of synaptic receptors by using microtransplantation of synaptic membranes (MSM)
- Cross-validate results of previous aims using publicly available RNA-Seq and in-situ hybridization datasets, to measure cellular and transcriptional E/I ratios.

Manuscript 2: Neuronal, synaptic and electrophysiological Excitatory to Inhibitory imbalance associates with loss of cognitive performances in Alzheimer's disease individuals

- Determine the *e*E/I ratio of synaptic receptors in MCI and AD subjects.
- Evaluate native synaptic receptor affinity to kainate and GABA
- Define whether synaptic proteins predict the *e*E/I balance
- Cross-validate results of previous aims in MCI and AD using publicly available RNA-Seq and in-situ hybridization datasets, to measure cellular and transcriptional E/I ratios.

- Investigate whether the E/I ratio across different levels of complexity correlate with cognitive impairment of the subjects.

CHAPTER 2. RESULTS

Increased functional Excitatory to Inhibitory synaptic ratio in parietal cortex of Alzheimer's disease subjects

In the present study, we utilized two complementary approaches to assess the global synaptic E/I ratio in the inferior PCx of AD subjects. The PCx is part of the DMN that is active during daydreaming, mind wandering, and introspection, but deactivates during demanding goal-directed cognitive tasks [76,96]. Importantly, baseline DMN activity is increased in AD and fails to deactivate during cognitive tasks, suggesting that the DMN is abnormally and continuously hyperactive in AD [97,98]. This may be due to disruptions in the E/I balance of principal neurons, although direct evidence is lacking. The present study was therefore undertaken to determine the anatomical E/I ratio in postmortem PCx from middle-aged subjects with AD, Down Syndrome (DS), and normal controls without pathology, using FDT to histologically assess the synaptic levels of markers for excitatory and inhibitory postsynaptic densities: postsynaptic density protein 95 (PSD-95) and gephyrin (GPHN), respectively. The DS group was included to compare synaptic effects in two neurological disorders with AD pathology; virtually all DS individuals exhibit AD pathology by 40 years of age [99]. The *e*E/I ratio was then measured by MSM isolated from slices adjacent to those used in FDT experiments. As originally described by Miledi and colleagues [100,101] , and expanded by others [102–104], the MSM technique allows for assessment of human receptors that are still associated with their natural lipid environment and accessory proteins. Results from the present work provide the first evidence that despite a loss of both excitatory and inhibitory synaptic proteins, individuals with AD exhibit a marked shift towards a pro-excitatory perturbation of postsynaptic densities and electrophysiological synaptic E/I balance. Further corroborating evidence for this

imbalance in AD PCx was found using publicly available RNA-Seq transcriptional datasets.

ANATOMICAL ALTERATIONS IN EXCITATORY AND INHIBITORY SYNAPTIC MARKERS IN CORTICAL LAYERS OF INDIVIDUALS WITH ALZHEIMER'S DISEASE PATHOLOGY

Quantitative FDT analyses were used to assess levels of PSD-95 and GPHN in parietal cortical layers 1 and 2 from individuals with AD or DS with AD pathology, and from normal controls (Figure 1). Both layers were assessed individually to test for differences in levels of the synaptic markers between the cell body-sparse layer 1 and the adjacent cell body-dense layer 2. Counts of PSD-95 and GPHN immunoreactive puncta in the sample fields from both layers were not significantly different across groups (Figure 1), indicating that the total density (puncta per volume) of excitatory and inhibitory synapses was maintained in PCx of middle-aged individuals including those in the disease states. Nevertheless, in all cases there was evidence of age-related pathology including an accumulation of large lipofuscin deposits often in association with GPHN immunopositive (+) cell bodies. In the AD cases we also observed dystrophic GPHN+ processes (Figure 1 d).

Next, we assessed the levels of immunoreactivity (ir) for both synaptic markers within individual synapse-sized puncta and plotted these measures in intensity frequency distributions (Figure 1 e-h). Both AD and DS cases were characterized by a reduction in the proportion of excitatory synapses with high levels of PSD-95-ir ($\geq$ 90 immunofluorescence intensity, on a 20-180 scale) and an increase in the proportion of excitatory synapses with lower intensity labeling. These changes were larger in the perikarya-rich layer 2 as compared to layer 1 (Figure 1 e, g); RM-ANOVA, $p < 0.0001$ for interaction between groups and intensities for both GPHN and PSD-95 in layer 2, vs $p = 0.0066$ for GPHN and $p = 0.0419$ for PSD-95 in layer 1. Consequently, the ratio of the high-to-low immunoreactivity for excitatory PSDs was significantly reduced in all AD and

DS cases (Figure 2 a-f). The leftward shift in intensity suggests that a larger proportion of excitatory synapses in AD and DS have smaller postsynaptic densities or disturbances in synaptic scaffolding. The intensity frequency distribution for analysis of GPHN-ir at inhibitory synapses demonstrated that changes in AD and DS cases were similar to those of PSD-95-ir (Figure 1 f, h), with there being a marked reduction in the ratio of high-to-low levels of GPHN-ir per synapse in both layers 1 and 2, and stronger effects in layer 2 (Figure 2 c-h). The disturbances in both PSD-95 and GPHN immunoreactivities suggest reductions in both excitatory and inhibitory drive in AD and DS, with effects being relatively greater in the vicinity of perikarya.

Given the marked reductions in levels of synaptic PSD-95-ir and GPHN-ir in both AD and DS groups, we next asked whether these proteins were similarly reduced or if they were differentially affected on a subject-by-subject basis. The ratio of the peaks of the immunolabeling frequency distributions for PSD-95 to GPHN (PSD-95-ir/GPHN-ir), for each subject, was not different between groups for layer 1 (Welch ANOVA allowing unequal variances, $p = 0.22$), indicating a similar anatomical E/I ratio for AD and DS versus controls (Figure 3 a). However, within layer 2 this ratio was significantly larger in the AD group as compared to controls (Welch ANOVA, $p = 0.0316$; followed by Dunn post hoc test comparing AD and DS vs control); the DS group had a trend in the same direction for layer 2 but this effect did not reach statistical significance due to greater group spread (Figure 3 b). These results suggest that while both PSD-95 and GPHN levels are reduced in AD, in layer 2 of PCx the ratio of excitatory to inhibitory postsynaptic elements is significantly elevated in AD versus controls.

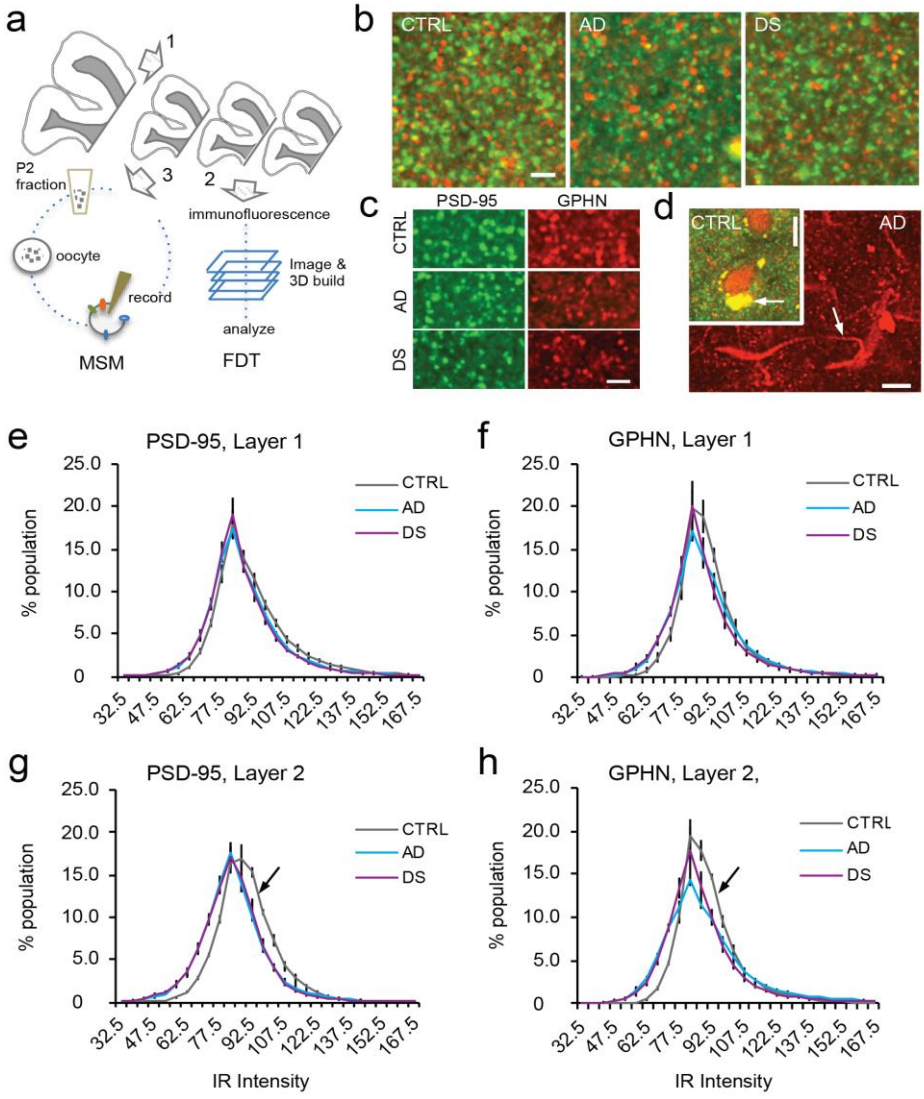

Figure 1 . Approach for analyses and quantification of changes in synaptic protein levels in AD and Down Syndrome (DS). **a,** Schematic illustrating the methodological approach for processing fresh-frozen parietal cortex subsections from the same tissue block (step 1) for either FDT (step 2) or MSM (step 3) analyses. See Methods for details. **b, c,** Photomicrographs showing PSD-95 (green) and GPHN (red) immunoreactive puncta in layers 1 (**b**) and 2 (**c**) parietal cortex from control (CTRL), AD, and DS subjects. Calibration bars, 2 µm (b & c). **d,** Examples of lipofuscin granules (arrow) surrounding GPHN immunopositive cells in a control case (inset, upper left; calibration bar, 10 µm), and GPHN+ dystrophic processes (arrow) in an AD case (calibration bar, 5 µm). **e, - h,** Synaptic immunolabeling intensity frequency distributions from the FDT analyses show the proportion of PSDs (Y-axis) in layers 1 (**e,f**) and 2 (**g,h**) that were immunolabeled for PSD-95 or *GPHN* at different intensities (X-axis) for the three groups; data plotted are group mean values ± SEM. Note the leftward skew in the immunolabeling intensity frequency distributions for the AD and DS groups relative to controls; this was most pronounced for layer 2 (RM-ANOVA, $p < 0.0001$ for interaction between groups and intensities for both *GPHN* and PSD-95 in layer 2; $p = 0.0066$ for *GPHN* and $p = 0.0419$ for PSD-95 in layer 1). Arrows in panels **g,** and **h,** indicate the control group which have a greater proportion of PSDs with high levels of the synaptic markers versus the AD and DS groups. Copied with permission from [129].

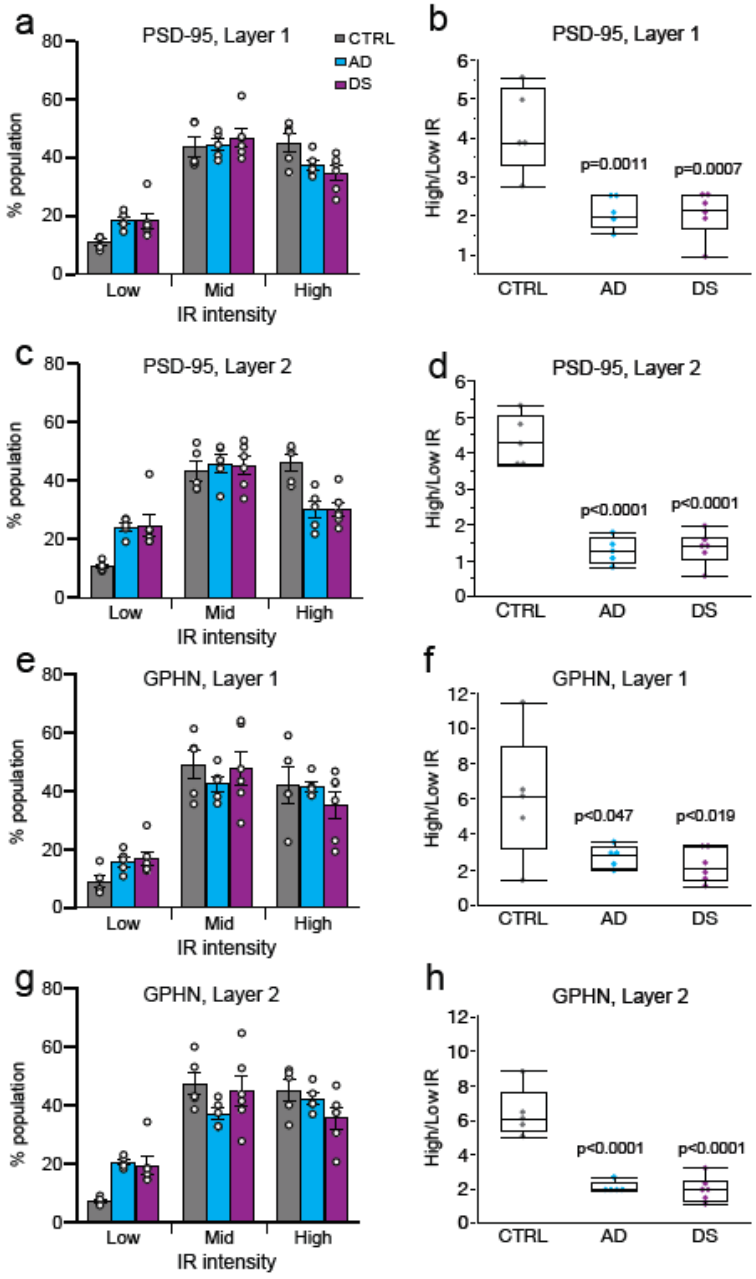

Figure 2. Levels of immunoreactivity for excitatory and inhibitory synaptic proteins are reduced in AD and DS. a,-d, Plots showing the proportion of PSD-95+ and GPHN+ puncta in each layer with immunofluorescence in low, mid or high intensity ranges for each group (group means ± SEM; based on Figure 1 **e, - h,** intensity distributions). RM-ANOVA (group x intensity interaction) indicated a significant effect for layer 2 only: $p = 0.0019$ for PSD-95 and $p = 0.0133$ for GPHN. RM-ANOVA for layer 1, $p = 0.1027$ for PSD-95 and $p = 0.4151$ for GPHN. (E-H) Box plots show the ratio of high-to-low labeling intensities for each individual case. As shown, all AD and DS cases exhibited significantly lower high-to-low intensity ratios as compared to controls for both postsynaptic proteins in each layer: PSD-95 layer 1, ($F(2,13) = 14.17$, $p < 0.0005$); GPHN layer 1 ($F(2,13) = 5.1$, $p < 0.023$); PSD-95 layer 2, ($F(2,13) = 8.4$, $p < 0.0045$); GPHN layer 2 ($F(2,13) = 37.54$, $p < 0.0001$). P values shown are from the Dunnett's post hoc test comparing AD or DS to control. Copied with permission from [129].

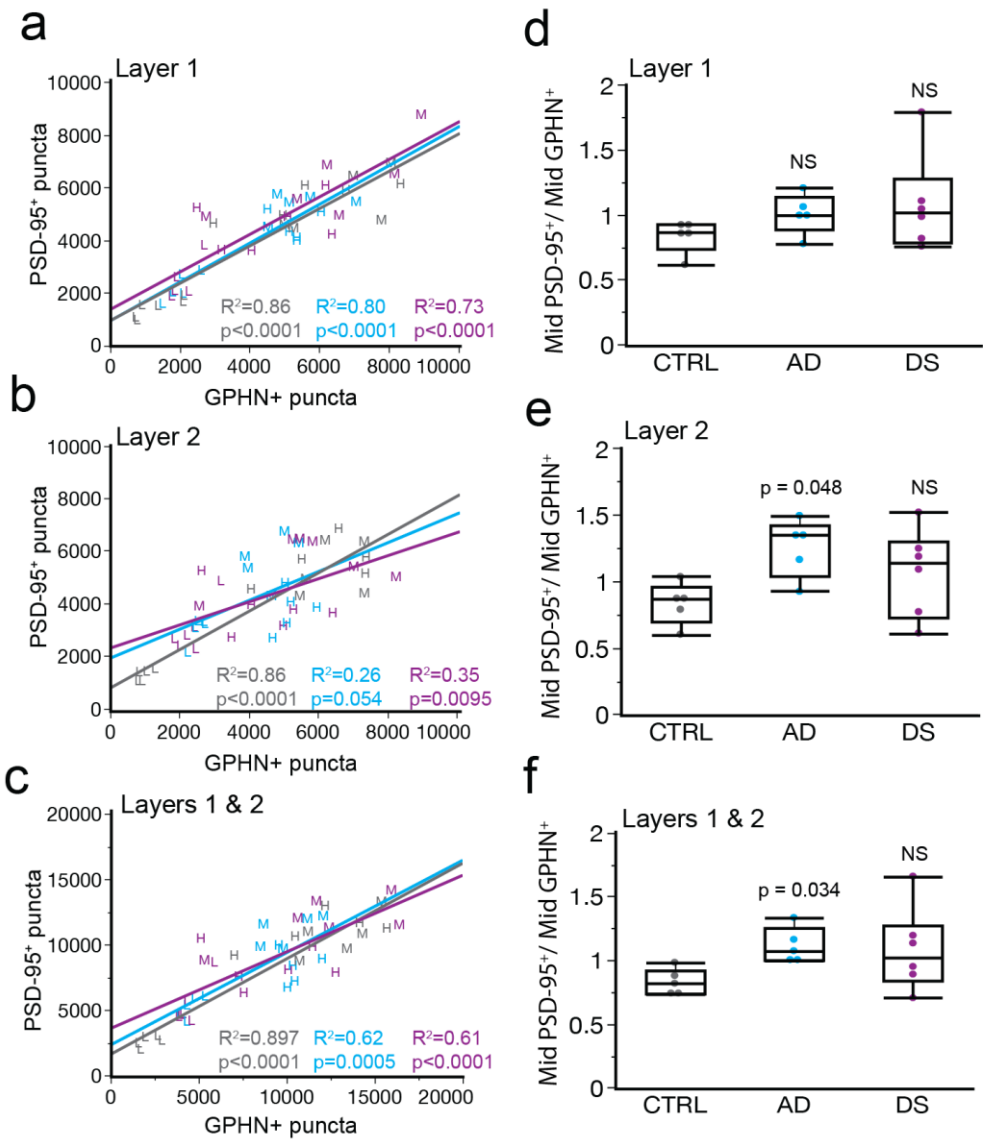

Figure 3. Differential alterations in the excitation-to-inhibition balance in parietal cortex of AD and DS. a, - c, Scatter plots show the ratio of the peak value from the PSD-95 intensity frequency distribution to the peak value from the GPHN distribution to provide a measure of the anatomical E/I balance for layers 1(**a.**) and 2 (**b**), and for the two layers combined (**c**.) **d - f,** As shown, the E/I balance (PSD-95/GPHN ratio) was not different between groups in layer 1 (a; Welch ANOVA allowing unequal variances p = 0.22), but it was significantly affected in layer 2 (b; Welch ANOVA; p = 0.0316) with only the AD group exhibiting elevated E/I balance versus controls (p =0.048, non-parametric Dunn's post hoc test). When layers 1 and 2 were combined, the difference between the AD and control groups was even greater (Welch ANOVA p = 0.0173; AD vs CTRL, p = 0.0336 Dunn's post hoc test). Notably, the DS group was highly variable in these E/I balance analyses. Copied with permission from [129].

REDUCTION OF SYNAPTOSOME-LIKE PARTICLES IN BOTH ALZHEIMER'S DISEASE AND DOWN SYNDROME

To determine whether the anatomical E/I synaptic marker protein alterations are indicative of alterations in the abundance of functional synaptic AMPARs and $GABA_A$Rs, P2 fractions enriched in synaptosomes were isolated from a single (20 µm-thick) cryostat section, adjacent to those used in FDT analysis, with the goal of recording the electrophysiological activity of synaptic receptors by MSM. As an intermediate step between FDT and MSM, one aliquot of the P2 fraction was examined by flow cytometry to aid in the interpretation of the immunohistochemical analysis from layers 1 and 2, and the global electrophysiological recording of synapses from the whole slice. Flow cytometry analysis showed a striking 48% and 64% reduction of synaptosome-like particles in the AD and DS groups, respectively, as compared to the control group ($F(2,13) = 15.82$, $p = 0.0003$; Figure 4 a, b). Aligning with the loss of synaptosome particles, total protein levels in the P2 fractions were also significantly reduced in the AD and DS groups ($F(2,13) = 21.5$, $p < 0.0001$) (Figure 4 b). The amount of protein and the number of synaptosomes were strongly positively correlated $R^2(16) = 0.75$; $p < 0.0001$.

These results indicate that preservation of the density of PSD-95+ and GPHN+ synapses in AD and DS, at least in superficial cortical layers, is at the cost of tissue shrinkage. We also observed a leftward shift in the size of recovered synaptosome-like particles from the AD and DS groups indicating that a large proportion of resilient synapses across all cortical layers have smaller-than-control sizes, a finding that is consistent with the reductions in immunoreactivity for both synaptic markers. Further in agreement with the FDT analyses, the ratio of large-to-small synaptosome-like particles was strongly reduced in AD and DS ($F(2,13) = 21.5$, $p < 0.0001$ vs control) (Figure 4 f), and the large/small ratio from the whole slice was linearly correlated to the high/low immunoreactivity for PSD-95 and GPHN in layers 1 and 2 combined ($R^2(16) = 0.69$, $p < 0.0001$) (Figure 4 g). Results from flow cytometry strongly suggests that synaptic deficits observed in cell-dense layer 2 identified with FDT are representative of effects in all cell-dense cortical layers, and that the P2 fractions capture those changes.

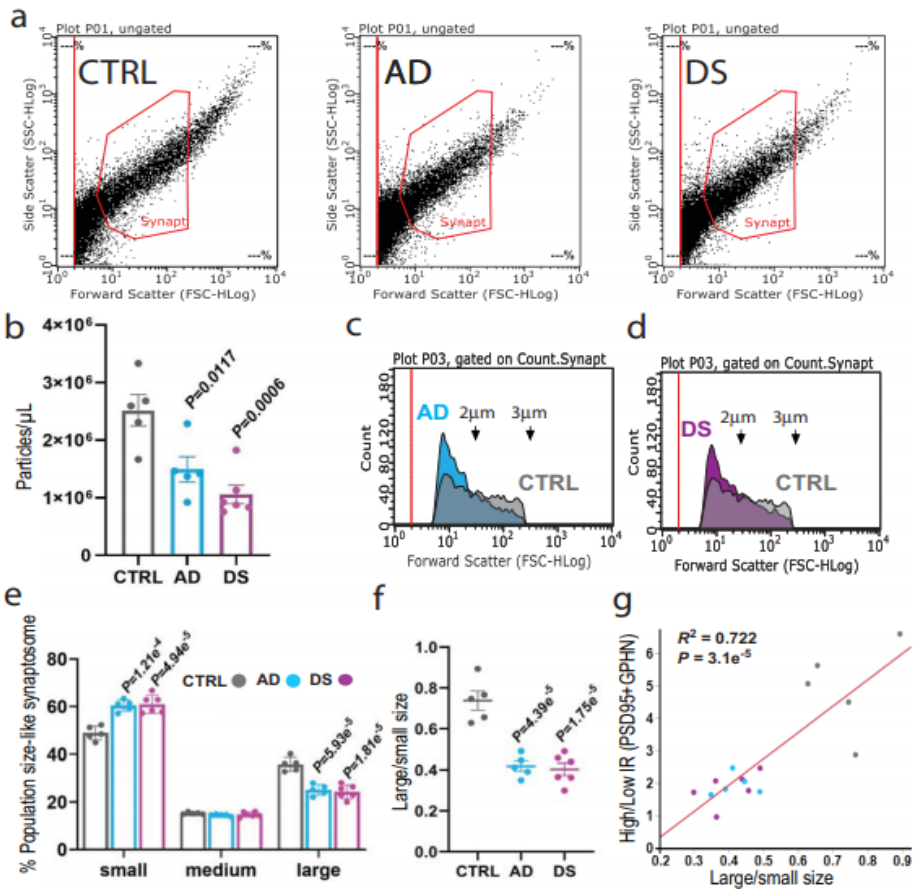

Figure 4. Flow cytometric analysis of synaptosomes in P2 fractions from AD and DS subjects. **a,** Representative plots indicate the gating parameters, based on size (1-5 um), used to quantify synaptosomes in P2 fractions from the parietal cortex of CTRL, AD and DS subjects. **b,** Numbers of particles within the size of synaptosomes were reduced from $1e^{+6} \pm 8.6\ e^{+4}$ in control (mean ± SEM; n = 5) to $5.2\ e^{+5} \pm 8.6\ e^{+4}$ in AD (n = 5) and $3.6\ e^{+5} \pm 7.9\ e^{+4}$ in DS (n = 6). An analysis of variance showed effect of diagnosis on particle count was significant, F (2,13) = 15.82, p = 0.0003. Post hoc analysis comparing to control using Dunnett's method (AD and DS vs CTRL) indicated that the average number of particles was lower in AD and DS. **c, d,** Forward scatter plots for synaptosome sized particles from AD and DS subjects compared to controls. Forward scatter plots are representative of particle size and show a shift to smaller size particles in AD and DS compared to control. **e.** Plots showing the proportion of particles within the size range of synaptosomes in P2 fractions that were further identified as being small (1 µm > diameter (∅) < 2 µm), medium (2 um ≤ ∅ ≤ 3 µm) or large (3 µm < ∅ ≤ 5 µm) sized for each group (group means ± SEM; based on c,d size distributions). ANOVA determined that effect of diagnosis was significant for large (F (2,13) = 18.88, p < 0.0001) and medium sized particles (F (2,13) = 16.7, p = 0.0003) but not for the small group (F (2,13) = 1.7, p = 0.2). **f,** All AD and DS cases exhibited significant reductions in the large-to-small size ratios for particles from P2 fractions (F (2,13) = 21.5, p < 0.0001). P values shown in the figures indicate the P value of the Dunnett's post hoc test comparing AD or DS vs control. **g,** Plot showing the correlation between FDT high-to-low immunoreactivity (IR) ratios (PSD-95-ir and GPHN-ir in layers 1 and 2 combined) and the large-to-small for each subject. Each subject is color coded by diagnosis: CTRL (gray), AD (cyan), DS (magenta). The solid line represents the Pearson's correlation; $R^2(15) = 0.692$, p < 0.000, showing agreement between intensity and size data from FDT and flow cytometry. Copied with permission from [129].

INCREASED ELECTROPHYSIOLOGICAL EXCITATORY TO INHIBITORY RATIO IN ALZHEIMER'S DISEASE BUT NOT DOWN SYNDROME.

Flow cytometry analysis identified a large reduction of synaptosome-particles in P2 fractions in AD and DS; this is in agreement with neuronal loss and synaptic dysfunction found in previous studies. To determine whether changes in postsynaptic markers are associated with changes in AMPARs and $GABA_A$Rs, we microtransplanted the same amount of synaptosomal membranes for each subject and measured the agonist-elicited responses of excitatory and inhibitory receptors in *Xenopus* oocytes. Because it is known that naïve oocytes (non-injected) do not express endogenous AMPARs or $GABA_A$Rs [105], the ion currents elicited by specific-agonists for these receptors in microtransplanted oocytes are mediated by the non-native human receptors. To confirm this point, in each experiment we tested agonists for AMPARs or GABAARs and were unable to elicit currents from non-injected oocytes, as we previously reported [106]. In contrast, oocytes microtransplanted with synaptosomes from each of the three groups, and clamped at a voltage of -80 mV, exhibited fast activated currents when perfused with 1 mM GABA (GABA currents) or 100 μM kainate (kainate currents) (Figure 5 a). As mentioned previously, kainate is an agonist of AMPARs that keeps the channel in a non-desensitized state, allowing steady-state measurement of AMPARs currents [107]. Co-perfusion of *s*-AMPA plus CTZ, after 3 min CTZ preincubation, elicited ion currents with similar amplitude of those produced by kainate alone (kainate vs AMPA+CTZ correlation: $R^2(16) = 0.935$, $p < 0.0001$) suggesting that kainate currents are mostly generated by AMPARs. To determine the contribution of kainate-type receptors specifically, we incubated microtransplanted oocytes in concanavalin A (ConA), a positive allosteric modulator of kainate-type receptors [108]. Figure 5 c shows no effect of ConA in this preparation, confirming that the contribution of kainate receptors in our recordings was negligible.

Having demonstrated agonist-induced responses in microtransplanted oocytes, we then tested for group differences. Maximal responses to GABA, kainate and AMPA+CTZ were variable across subjects (Figure 5); this was most striking in the DS group, which included some of the largest ion currents recorded. Therefore, although both AMPAR and $GABA_A$R responses tended to be smaller in AD versus control cases, the differences were

not statistically significant. It is important to note that this study was not powered to detect differences in the total amplitude of the currents when measured individually (Figure 5 b). However, the maximal amplitude of currents through AMPARs and GABAARs were highly correlated across subjects (Figure 5 d, e). Because the correlation between ion currents elicited by kainate and GABA ($R^2(16) = 0.942$, $p < 0.0001$) was higher than that between s-AMPA+CTZ and GABA ($R^2(16) = 0.916$, $p < 0.0001$), we used kainate and GABA currents to calculate the *e*E/I ratio for each subject. For this, measures were collected and averaged only from oocytes in which both kainate and GABA currents measured show a response:noise ratio equal or higher than 3. As compared to controls, only the AD group exhibited an increase in electrophysiological E/I balance with the kainate/GABA response ratio being significantly greater than for controls ($F(2,13) = 4.21$, $p < 0.0387$; Figure 5 f); responses from the DS group did not differ from controls. Combined with results from the FDT and flow cytometry analyses, these findings provide the first evidence that individuals with AD have a shift in the E/I balance leading to greater excitatory relative to inhibitory activity in cortex compared to that observed in controls.

Unlike the AD cases, the *e*E/I ratio was preserved in DS (vs controls) despite these individuals exhibiting severe plaque and tangle pathology that was comparable to the AD group. As described above, the DS group exhibited large variability in ion currents that lead us to ask whether this might reflect another aspect of pathology such as levels of phosphorylated (p) tau, which can vary across individuals despite similar AD staging [109]. Thus, we tested if ion currents in the DS group were correlated with ptau levels. Notably, in DS individuals the amplitude of kainate currents was negatively correlated with ptau levels ($\rho(6) = -0.9429$, $p = 0.0048$; non-parametric Spearman's ρ to avoid artifactual correlations due to extreme variability). In addition, the numbers of synapses with high levels of PSD-95-ir (layers 1 and 2 combined) were also negatively correlated with AT8-ir denoting ptau levels ($\rho(6) = -0.8857$, $p = 0.0188$). Neither the amplitude of GABA currents ($\rho = -0.7714$, $p = 0.07$) nor GPHN-ir per synapse ($\rho = -0.09$, $p = 0.87$) was significantly correlated with ptau levels. For the AD subjects, ptau levels did not correlate with either measure ($p > 0.2$ for all) likely reflecting the small within-group difference in ptau levels.

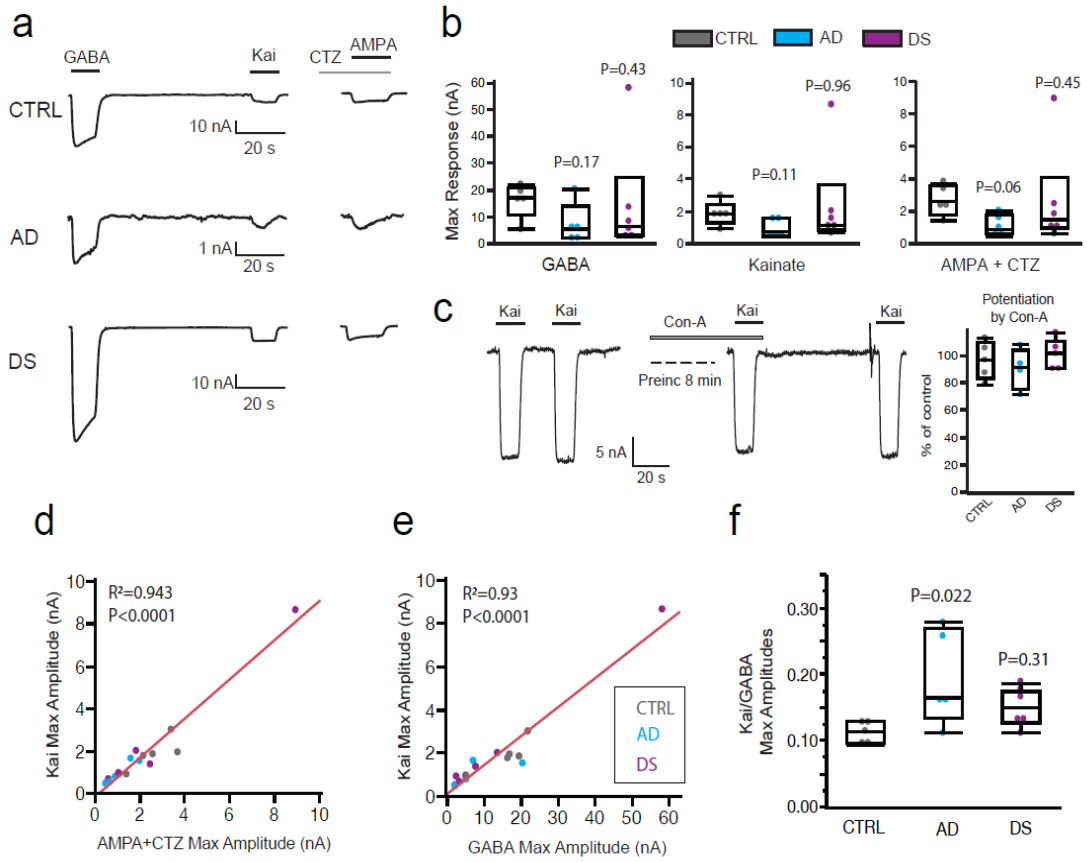

Figure 5. Differential alterations of the excitation to inhibition balance in ion currents of microtransplanted receptors from AD and DS parietal cortex. **a,** Functional responses of microtransplanted synaptic receptors were elicited by application of 1 mM GABA, 100 µM kainate, or 10 µM s-AMPA in combination with 10 µM cyclothiazide (CTZ), after 3 min preincubation with CTZ. **b,** No significant group differences were found in the maximal amplitude of agonist-induced ion currents for any of the responses (Welch ANOVA allowing unequal variances $p = 0.27$ for kainate, $p = 0.09$ for AMPA+CTZ, $p = 0.34$ for GABA). The DS group had both the largest, and some of the smallest, responses indicating a large within-group data spread in this condition. **c.** Kainate-induced responses were not potentiated by concanavalin A (Con-A), a positive allosteric modulator specific for kainate-type glutamate receptors, indicating that the participation of kainate receptors is negligible and kainate-induced receptors are generated by AMPA-type receptors. **d, e,** Plots showing the correlation between responses of excitatory receptors activated by kainate or AMPA plus CTZ and those of inhibitory receptors activated by GABA. Each point represents the average of responses from three recordings sessions. The solid lines represent the Pearson's correlation. **f,** Excitation to inhibition ratio, defined as the average of maximum amplitude of kainate- to GABA-induced currents measured from the same oocyte was significantly larger in oocytes microtransplanted with synaptic membranes from AD compared to control brains ($F(2,13) = 4.2$, $p < 0.0387$). P value in plot indicates results from Dunnett's post hoc test. Copied with permission from [129].

INCREASED TRANSCRIPTOMIC *DLG4/GPHN* RATIO IN ALZHEIMER'S DISEASE.

To determine whether the E/I imbalance in AD is reflected at the transcriptional level in a larger independent cohort, we used publicly available RNA-Seq data from the Aging, Dementia and Traumatic Brain Injury (ADTBI) cohort to calculate the transcriptional E/I ratio in PCx. The transcriptional E/I ratio was defined as the level of mRNA for *DLG*4, which encodes PSD-95, divided by the level of mRNA for *GPHN*, which encodes gephyrin. An effect of clinical diagnosis ($p = 0.00891$) was found on *DLG*4/*GPHN* ratios when individuals were pooled by signs of dementia (AD type by DSM-IV clinical DX) or non-dementia (Figure 6 a). Ageing had no effect ($p = 0.34566$).

Taking all these results together, using multiple approaches, we report here the first evidence for a shift of the global E/I synaptic balance in the inferior PCx of the AD brain that favors greater synaptic excitation. While results from FDT studies indicate a reduction in levels of both excitatory and inhibitory synapse markers of middle-aged AD subjects, the ratio of PSD-95 to GPHN was strikingly altered in layer 2, indicating greater excitatory connectivity in this region. Gene expression analyses for PSD-95 and GPHN transcripts, in a larger cohort of subjects with level of pathology similar to the ones used in FTD studies, provided additional evidence for a shift in E/I imbalance, and suggest that alterations in layer 2 may extend to other cell-dense layers in the PCx. Electrophysiological recordings from MSM studies also showed unequal deficits in postsynaptic AMPAR- and $GABA_AR$-mediated ion currents, leading to an increase in the global electrophysiological synaptic E/I ratio, which would favor enhanced synaptic excitatory drive. The E/I shift in AD is remarkable in the context of studies showing that synaptic levels of inhibition are generally proportional and scaled in strength to excitation, despite even large variations in the amplitude of excitatory synaptic currents across neurons [81,88,110]. Changes in excitatory synapse number and/or strength predicted for Hebbian plasticity during learning and memory is similarly compensated for by synaptic scaling [111], heterosynaptic plasticity [110], and changes in synaptic function within minutes and hours [112]. Indeed, the E/I ratio in our MSM study had minimal variation compared to ion currents measured individually,

indicating that on average the relationship between postsynaptic AMPARs and $GABA_ARs$ is nearly constant in control individuals, and even in DS.

Our converging evidence suggests that a pro-excitatory synaptic imbalance may underlie the hyperexcitability and reduced resting state deactivation that have been consistently observed in the PCx of AD patients [113,114]. Further dissection of the transcriptional E/I ratio by amyloid plaque burden severity indicated that those with severe amyloid deposition and dementia had larger transcriptional E/I ratios than those without these clinical manifestations. This suggests that homeostatic mechanisms that maintain the E/I ratio are preserved in so-called "resilient" individuals that remain cognitively intact despite abundant Aβ plaques and NFTs [115,116]. Importantly, people with dementia but without amyloid deposition also had significantly larger transcriptional E/I ratios compared to controls. These results suggest that pro-excitatory E/I ratios primarily correlate with dementia status, with potential secondary effects reflecting the level and type of pathology. Thus, cortical hyperexcitability may be part of a positive feedback loop whereby higher neuronal activity promotes production and accumulation of toxic Aβ and Tau oligomers [95] resulting in unequal synaptic losses that, in turn, lead to greater excitation. The preservation of a normal synaptic E/I balance in PCx in DS is an interesting finding. To our knowledge whether the default mode network shows signs of hyperactivity in DS is not known. However, comparative imaging studies of DS and control subjects did not find functional differences in the resting-state connectivity within PCx, even in subjects with APOE ε4 vs APOE ε3 variants that denote a higher risk for AD [117], suggesting resilience or persisting homeostatic mechanisms in this region in DS despite AD-like pathology.

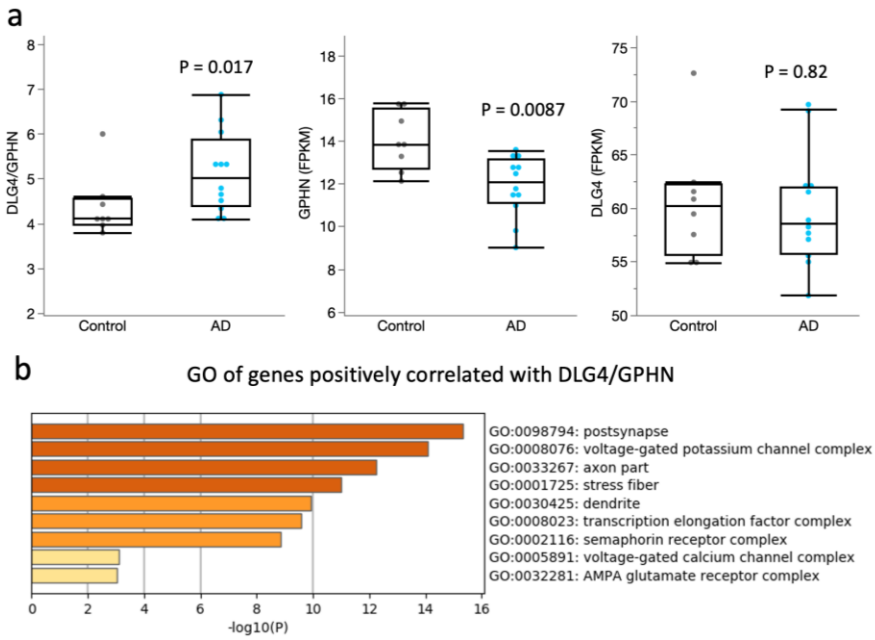

Figure 6. Differential alterations in expression of excitatory and inhibitory postsynaptic density proteins are associated with dementia in AD. **a,** The transcriptional E/I ratio for *DLG*4 to *GPHN* (*DLG4*/*GPHN*) using RNA-Seq datasets from the Aging, Dementia and Traumatic Brain Injury study (ADTBI), was significantly increased in AD cases compared to controls with no pathology (n = 8 cognitive healthy controls, CERAD = 0 and 12 subjects with a DSM-IV clinical diagnosis of dementia of the AD disease type and AD pathology CERAD = 3). The difference was driven by reduction in *GPHN* expression and not from *DLG*4, p value from the non-parametric Wilcoxon test. **b,** Top representative clusters of the gene ontology (GO) analysis for cellular component of genes positively correlated with the *DLG*4/*GPHN* ratio implemented in Metascape. Copied with permission from [129] .

ELEVATED EXCITATORY TO INHIBITORY NEURONAL RATIO IN ALZHEIMER'S DISEASE.

To further elucidate sources of E/I balance disruption in the PCx in AD, we used publicly available in situ hybridization image data from the ADTBI study [118], to quantify the number of glutamatergic neurons that expressed mRNA for the excitatory vesicular glutamate transporter 1 (vGluT1) and GABAergic neurons that expressed mRNA for GABA transporter 1 (GAT1), in a well-defined area of the cortex. For this, $vGluT1+_{mRNA}$ and $GAT1+_{mRNA}$ cells in PCx layers I-VI were counted (Figure 7 a, b) and their densities (number of cells/ area) in AD compared to controls. Densities of $vGluT1+_{mRNA}$ cells were not different between groups ($p = 0.6$, Wilcoxon test) (Figure 7 c). In contrast, densities of $GAT1+_{mRNA}$ cells were significantly reduced in AD ($p = 0.015$; Figure 7 c). Comparing the ratios of vGluT1 to GAT1 expressing cells for each case demonstrated a marked increase in this cellular E/I ratio in the AD group ($p = 0.0026$; Figure 7 d). Importantly, the *DLG4*/*GPHN* ratio that represent postsynaptic elements (Figure 6 b) was linearly correlated with the E/I cell ratio, and the correlation was driven by changes in the AD group. These results support the conclusion that the synaptic changes in PSD-95 and GPNH in AD are among more widespread cellular changes including marked decreases in GABAergic neurons expressing GAT1 that contribute to the shift in E/I balance in the PCx of AD patients.

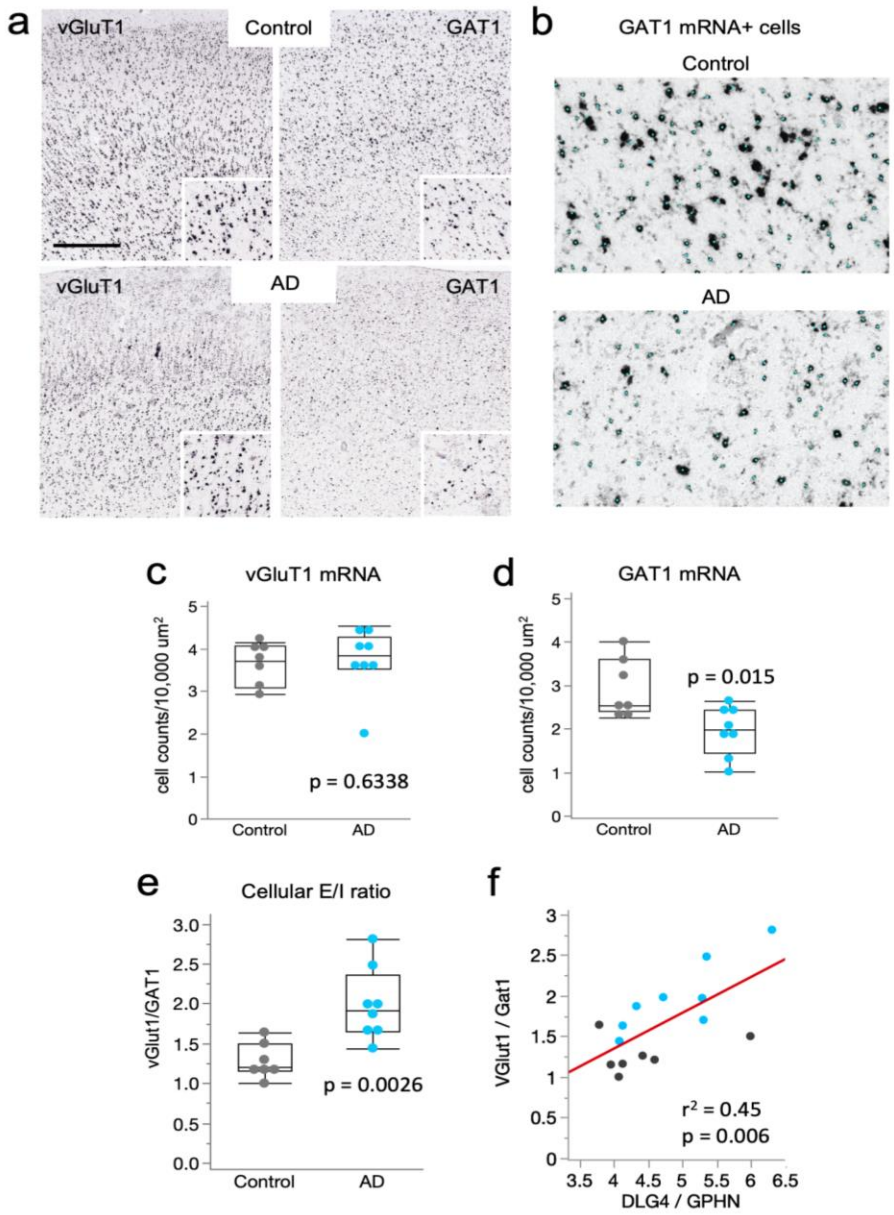

Figure 7. Marked reductions in GAT1 mRNA expressing cells in AD cases. **a,** Images showing colorimetric in situ hybridization for vGluT1 and GAT1 mRNAs in a control no dementia-CERAD 0 case and a dementia-CERAD 3 AD case. Insets show labeled cells at higher magnification. Calibration bar, 750 µm; 375 µm for inset. **b,** Images showing examples of GAT1 mRNA positive (+) cells that were identified and counted in the analyses; identified cells are overlaid with a small cyan dot. **c, d,** Quantification of vGluT1 and GAT1 mRNA expressing cells in parietal cortex per 10,000 µm2 (plots show median values, 25th and 75th percentiles, and minimum and maximum range). GAT1 expressing cells were reduced in the AD dementia-CERAD 3 group (n = 8) versus the control, no dementia-CERAD 0 group (n = 7). P values are from the Wilcoxon Test. **e,** vGluT1/GAT1 ratios for the same subjects. The cellular E/I ratio was significantly elevated in the AD group versus controls (**p < 0.01). **f,** Linear correlation between the cellular (vGluT1/GAT1) and transcriptional (DGL4/*GPHN*) expression E/I ratios for cases with both data sets; AD cases, cyan; control cases, black. Copied with permission from [129].

Neuronal, synaptic and electrophysiological Excitatory to Inhibitory imbalance associates with loss of cognitive performances in Alzheimer's disease individuals

We determined the E/I ratio across different layers of complexity in the postmortem human TCx and hippocampus from non-demented controls, MCI and AD subjects. TCx and hippocampus are areas early affected by AD, are among the most studied in AD research and their level of hyperactivity correlate with the decline of cognitive performance in subjects at risk of AD [119]. We found convergent evidence of cortical pro-excitatory changes, driven by loss of GABAergic synapses and neurons, that strongly correlate with overall and discrete metrics of cognitive performance in AD.

DISCRETE ELECTROPHYSIOLOGICAL METRICS OF SYNAPTIC FUNCTION ARE CORRELATED WITH DISEASE SEVERITY.

To test the hypothesis that hippocampus and TCx in AD are characterized by functional impairment of the synaptic E/I balance, we first prepared P2 fractions from hippocampi tissue of 8 cognitively normal subjects with no AD pathology (CTRL), 8 MCI and 8 AD subjects, as well as the TCx from 6 CTRL, 6 MCI and 6 AD subjects. Size-gated synaptosome-like particles were first counted by flow cytometry using specific antibodies against the postsynaptic densities PSD-95 for excitatory synapses and GPHN for inhibitory ones. Then, we performed MSM experiments to determine the *e*E/I ratio. As before, the *e*E/I ratio was defined as the maximum amplitude of AMPARs current divided by the peak amplitude of $GABA_A$Rs current in the same microtransplanted cell (oocyte).

We observed a significant reduction in the number of labeled and size-gated synaptosome like particles from the TCx of MCI and AD compared to the CTRL subjects in our synaptosome preparations (Figure 8), indicating an early synaptic loss in MCI driven by the loss of PSD-95 labeled synapses. Surprisingly, no differences in the hippocampus across diagnostic groups was observed (Figure 8).

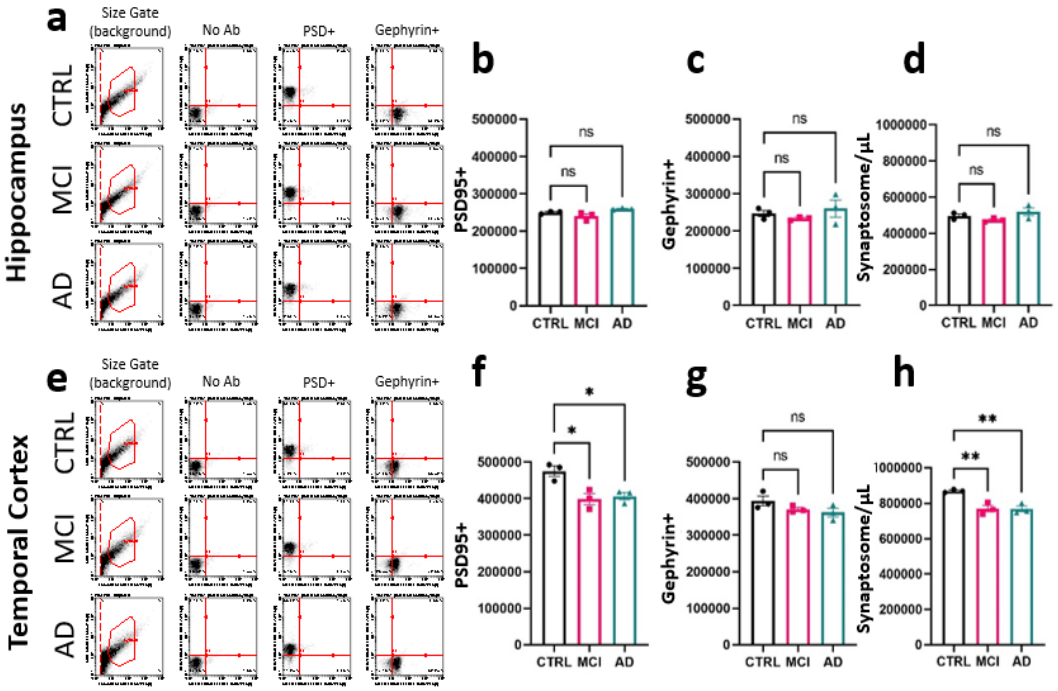

Figure 8. Reduction of the synaptosome counting in MCI and AD temporal cortex. a, e, representative flow cytometer plots of CTRL, MCI and AD pools of hippocampus (top) and TCx (bottom). We analyzed synaptosome particles using side scatter/forward scatter. Size-gate plots were build using size beads to include synaptosome size-like particles and excluding background particles. We further analyzed synaptosome size-like particles positive for PSD95 or GPHN antigen (as described in the methods section). **b, f,** Excitatory synaptosomes were significantly reduced in TCx of MCI and AD compare to CTRL (one-way ANOVA, $F(2, 6) = 10.03$, $p = 0.01$ followed by Dunnett multiple comparison test, MCI $p = 0.01$, and AD $p = 0.02$). In hippocampus, MCI and AD did not show the same reduction compare to CTRL (one-way ANOVA, $F(2, 6) = 6.28$, $p = 0.03$ followed by Dunnett multiple comparison test MCI $p = 0.26$, AD $p = 0.25$), however, MCI was reduced compare AD (Tukey multiple comparison AD vs MCI $p = 0.03$). **c, g,** Number of positive synaptosome for GPHN did not change among diagnosis groups in hippocampus (one-way ANOVA, $F(2, 6) = 0.89$, $p = 0.46$) and TCx (one-way ANOVA $F(2, 6) = 2.32$, $p = 0.18$). **d, h,** Overall, we observed a significant reduction in total number of synaptosomes in TCx of MCI and AD compared to the CTRL (one-way ANOVA $F(2, 6) = 15.04$, $p = 0.005$ followed by Dunnett's multiple comparisons test CTRL vs MCI $p = 0.006$; CTRL vs AD $p = 0.005$), but no differences in hippocampus across diagnostic groups (one-way ANOVA $F(2, 6) = 2.57$, $p = 0.16$). Whiskers represent standard errors. * indicates a p value < 0.05; ** indicates a p value < 0.01.

Aliquotes from these preparations were used for MSM experiments. Microtransplanted oocytes effectively inserted human native membranes containing functional synaptic AMPARs and $GABA_A$Rs (Figure 9). Although, oocytes microtransplanted with AD membranes had a more depolarized resting membrane potential compared to those injected with MCI samples, probably due to pore-forming oligomeric

Aβ present in P2 fractions [120,121] (Figure 9), no statistically significant difference in the maximum amplitude of ion currents elicited by the activation of synaptic receptors was observed in both brain regions (Figure 9). Importantly, AMPARs and $GABA_A$Rs currents from hippocampus and TCx were highly correlated indicating a strong regulation of the global E/I ratio (Figure 10). The *e*E/I ratio was not different across diagnosis in the hippocampus (Figure 9), but it was significantly higher in the TCx of AD subjects (Figure 9). To explore the relationship between receptor function and overall cognitive performance we correlated first the amplitude of currents elicited by microtransplanted synaptic receptors with the score from MMSE (cognitive test briefly described in the chapter 1, it is commonly used as part of the evaluation for possible dementia)[122]. In the hippocampus, the higher the amplitude of $GABA_A$Rs currents the better the cognitive performance was (Figure 11b). A similar association was observed for AMPARs currents (Figure 11c). In the TCx, neither $GABA_A$Rs nor AMPARs currents correlated with the MMSE (Figure 11 f-g). We also correlated the *e*E/I ratio with MMSE scores. Whereas the hippocampal *e*E/I ratio had no correlation with MMSE (Figure 11 d), the *e*E/I ratio in the TCx was negatively associated with the MMSE (Figure 11 h). Interestingly, we also observed that the larger the abundance of neuritic plaques (CERAD) or tangles (Braak stage) in the TCx the larger the *e*E/I ratio (Figure 11 k-l), but not in the hippocampus (Figure 11 i-j). We further investigated whether the *e*E/I imbalance found in TCx, or the lack of it in hippocampus, was due to differences in the pharmacological affinity of synaptic receptors. Concentration-response curves for AMPARs and $GABA_A$Rs currents did not show differences on their EC_{50} across groups in hippocampus (Figure 12 a,b) and TCx (Figure 12 c,d) indicating that the alterations of the *e*E/I ratio in the TCx of AD subjects was not due to changes in receptor affinity.

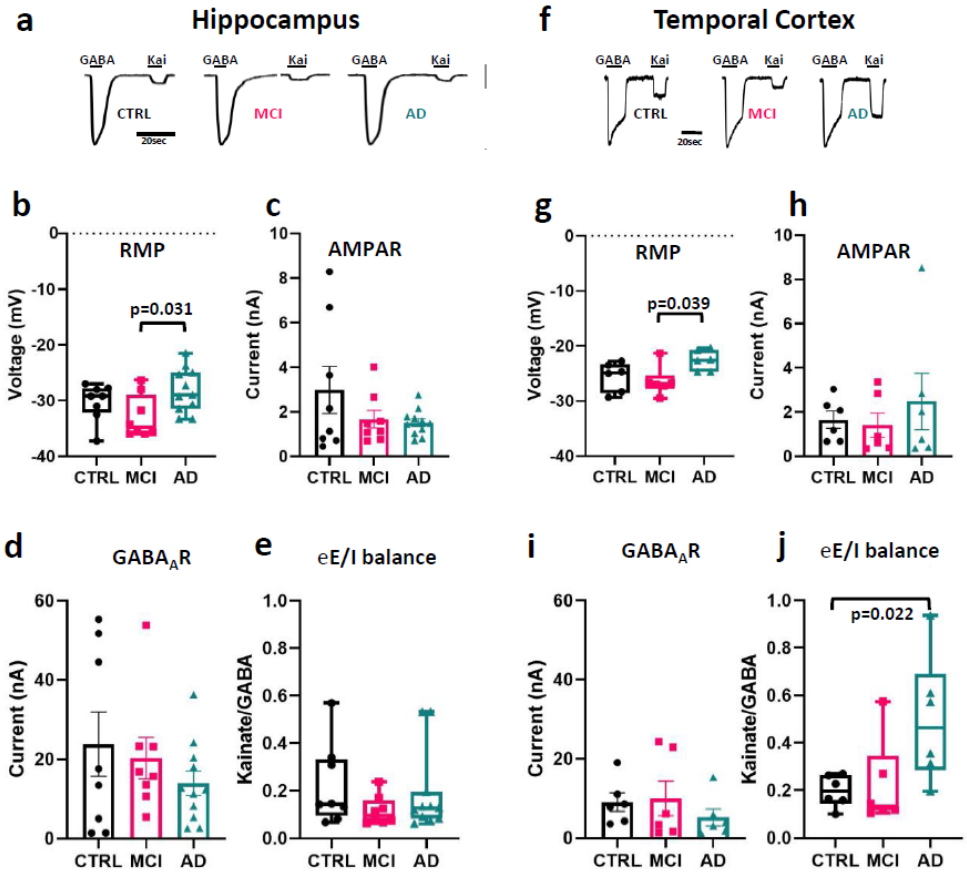

Figure 9 Pro-excitatory perturbation of *e*E/I balance in TCx of AD subjects, but not in hippocampus. **a, f,** Representative electrophysiological responses from oocytes microtransplanted with human synaptic membranes from hippocampus or TCx, perfused with 1mM GABA and 100 µM kainate, an agonist of AMPAR. **b, g,** Resting membrane potential (RMP) of oocytes microtransplanted with human membranes were different across diagnostic groups in hippocampus (one-way ANOVA F (2, 24) = 3.7091, p = 0.039) and TCx (one-way ANOVA F (2, 15) = 4.0846, p = 0.038). Multiple comparisons test shows that the RMP in oocytes with membranes from hippocampus and TCx were more depolarized in AD compared to MCI (hippocampus post-hoc Tukey p = 0.031; TCx post-hoc Tukey p = 0.039). **c, h,** AMPAR responses to kainate were not significantly different across diagnostic groups (hippocampus: one-way ANOVA - F (2, 24) = 1.7785, p = 0.19; TCx: one-way ANOVA - F (2, 15) = 0.45762, p = 0.64). Each point in the plot is the average of the maximum AMPAR responses to kainate per subject. **d, i,** $GABA_AR$ responses to GABA did not show differences within diagnostic groups (hippocampus: one-way ANOVA - F (2, 24) = 0.91111, p = 0.42; TCx: one-way ANOVA - F (2, 15) = 0.66370, p = 0.53). **e, j,** *e*E/I was increased in TCx (one-way ANOVA F (2, 15) = 4.5791, p = 0.028 followed by Dunnet's test p = 0.022 and Tukey's test p = 0.039) but no in hippocampus (one-way ANOVA F (2, 24) = 1.0913, p = 0.35). The *e*E/I balance was calculated from the near-simultaneous recording of maximum responses of AMPAR and $GABA_AR$ in every single oocyte. Each point is the average of at least 3 oocytes per subject, from 6 (hippocampus) or 5 (TCx) independent experiments. In the bar chart of **c, d, h,** and **i,** lines show standard error; in **e,** and **j,** the boxes extend from the 25th to 75th percentiles and the whiskers extend down to the minimum and up to the maximum value.

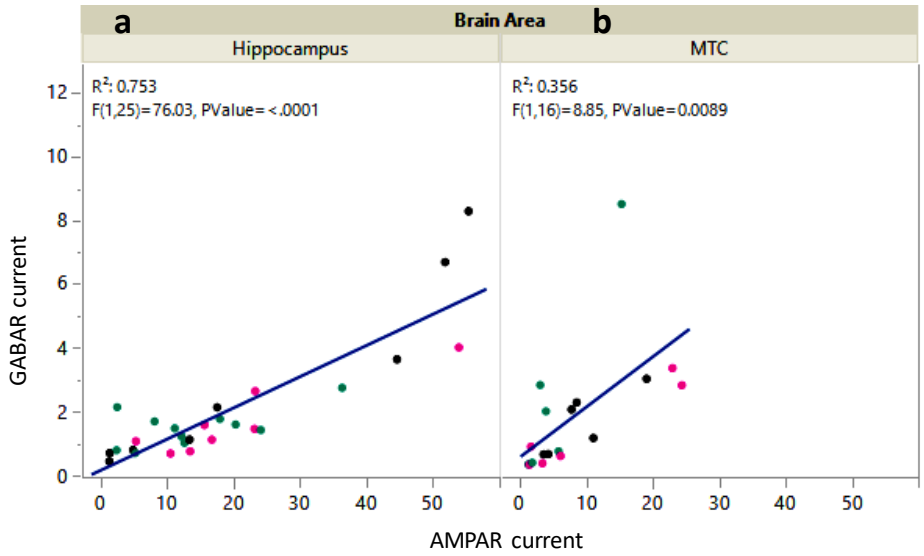

Figure 10 Global synaptic excitatory and inhibitory ratio is highly stable within the same brain area. Microtransplanted oocytes with **a,** hippocampus or **b,** TCx synaptosome fractions from CTRL (black), MCI (magenta) and AD (aqua) subjects, were tested with 1mM GABA and 100µM kainate eliciting $GABA_AR$ and AMPAR currents, respectively. $GABA_AR$ and AMPAR currents correlate suggesting that electrophysiological synaptic E/I balance is stable within the same area of the brain.

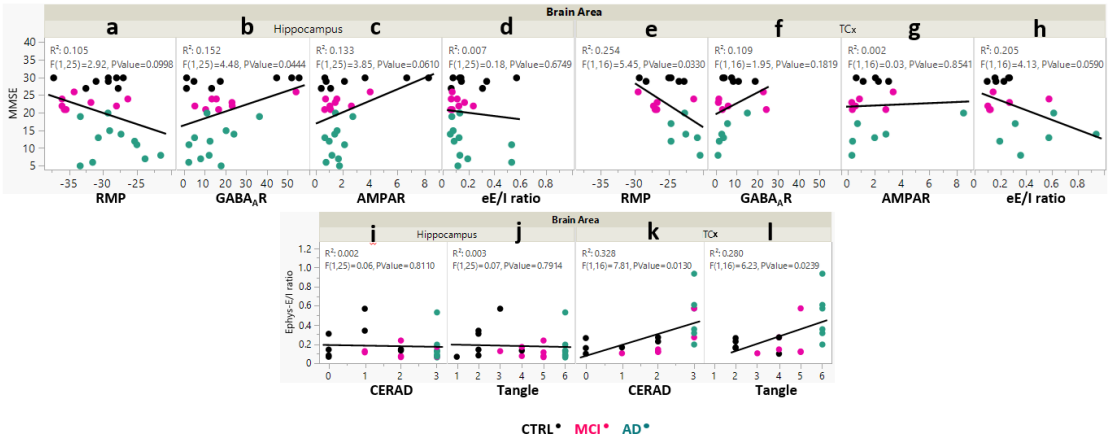

Figure 11. Pearson's correlations between synaptic receptors currents, E/I ratio, oocytes' resting membrane potential and MMSE scores in each diagnostic group in hippocampus and MTC. a, e, Resting membrane potential negatively correlates with MMSE in TCx, but not in hippocampus. In hippocampus, the higher the amplitude of $GABA_AR$ current the better was the cognitive performance of the subject (MMSE) (**b**). A similar trend was observed for AMPAR currents (**c**). In the TCx neither $GABA_AR$ nor AMPAR currents correlated with the MMSE (**f, g**). Whereas the *e*E/I ratio had no correlation with MMSE in the hippocampus (**d**), there was an association between the eE/I ratio and MMSE in the TCx (**h**). **i-l**, *e*E/I ratio (AMPA/GABA). Whereas the *e*E/I ratio had no correlation with MMSE in the hippocampus, there was an association between the eE/I ratio and MMSE in the TCx.

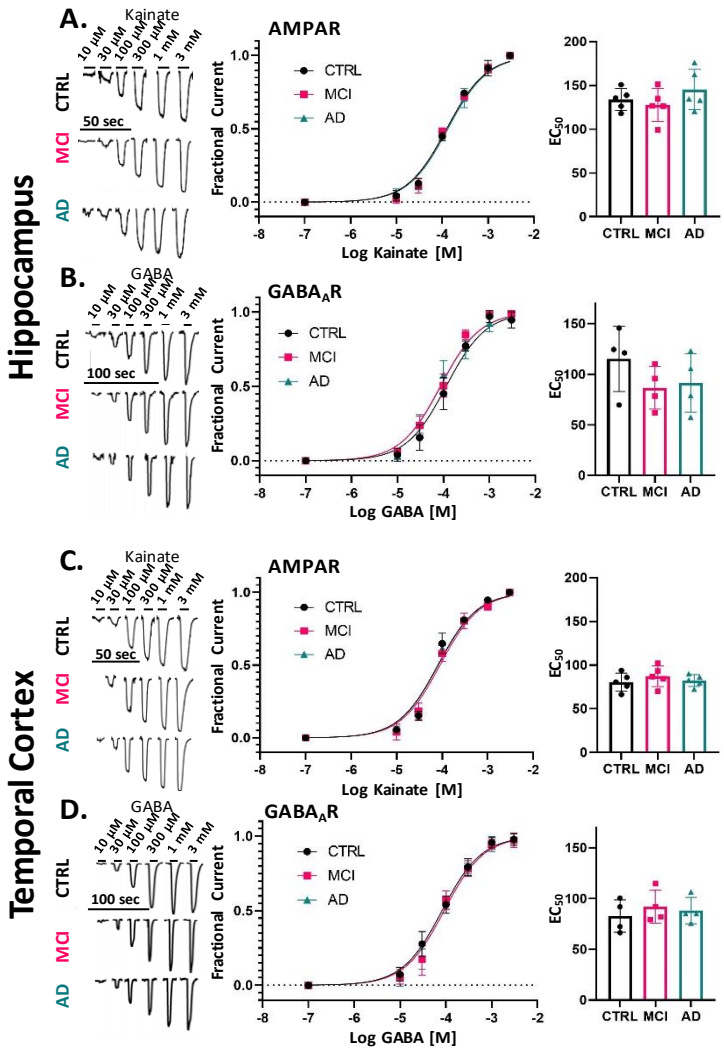

Figure 12 Preservation of synaptic receptor affinity in TCx and hippocampus. a, c, Left panels, representative recording of currents elicited by different concentrations of kainate (from 100nM to 3mM) on microtransplanted oocytes with a pool of synaptosome fraction from hippocampus and TCx of CTRL (hippocampus = 8; TCx = 6), MCI (hippocampus = 8; TCx = 6) and AD (hippocampus = 11; TCx = 6) subjects. **a, c,** central panels, kainate activating AMPAR dose–current response relationships, (hippocampus = 5 and TCx = 5 oocytes). **a, c,** right panels, EC_{50} obtained from AMPAR dose-response did not show differences in both hippocampus (one-way ANOVA F (2, 12) = 1.1578, p = 0.35) and TCx (one-way ANOVA F (2, 12) = 0.63501, p = 0.55). **b, d,** left panels, currents elicited by different concentrations of GABA (from 100nM to 3mM) on microtransplanted oocytes with a pool of synaptosome fraction from hippocampus and TCx of CTRL (hippocampus = 8; TCx = 6), MCI (hippocampus = 8; TCx = 6) and AD (hippocampus = 11; TCx = 6) subjects. **b, d,** central panels, GABA activating $GABA_AR$ dose–current response relationships, (hippocampus = 4 and TCx = 4 oocytes). **b, d,** right panels, EC_{50} obtained from $GABA_AR$ dose-response did not show differences in both hippocampus (one-way ANOVA F (2, 9) = 0.37050, p = 0.70) and TCx (one-way ANOVA F (2, 9) = 1.2239, p = 0.34). For all figures, the oocyte membrane potential was held at −80 mV. Data were collected from two independent experiments and all values were normalized to the maximum. Whiskers from each dose point represent standard deviations.

ELECTROPHYSIOLOGY-ANCHORED ANALYSIS OF THE SYNAPTOPROTEOME AND ITS CORRELATION WITH SYNAPTIC RECEPTOR ACTIVITY, NEUROPATHOLOGY AND COGNITIVE PERFORMANCE

To investigate alternative causes for the increased *e*E/I ratio in the TCx, we evaluated the abundance of proteins in the TCx synaptosome preparations using nanoflow liquid chromatography-tandem mass spectrometry (nanoLC-MS/MS). We found a total of 2900 proteins from which 96% (2788 proteins) were expressed by the three groups. We first focused on proteins for the subunits composing the pore of AMPARs and $GABA_AR$s present in our preparations. Since subunits for these receptors were part of the heteromeric receptors present *in vivo*, and they have strong complementary relationships among members of their own family [123,124], we analyzed whether the sum of all AMPAR subunits (ΣAMPARs) correlated with the sum of all $GABA_AR$ subunits (Σ$GABA_AR$s) and whether there were differences across groups. As expected from our electrophysiological results, ΣAMPARs and Σ$GABA_AR$s were strongly correlated (Figure 13 a); however, no differences in their abundance, or their ratio (Figure 13 d) were found across groups. No differences were also observed for the synaptic scaffolds PSD-95 or GPHN or the proteomic ratio (*p*E/I ratio) defined as PSD-95/GPHN (Figure 13 e). Notably, the abundance of AMPAR subunits correlated with the electrophysiological amplitude of AMPARs currents and PSD-95 (Figure 13 f); however, the abundance of $GABA_AR$ subunits did not correlate with the amplitude of $GABA_AR$s responses or GPHN (Figure 13 g). The loss of correlation between the protein and function of inhibitory $GABA_AR$s drives the dissociation between the *e*E/I ratio and the *p*E/I ratio (Figure 13 b). Because the electrophysiological function of AMPARs and $GABA_AR$s is strongly modulated by auxiliary proteins we further screened for proteins correlated ($p < 0.05$) with the amplitude of the currents elicited by these receptors [125]. We found 495 proteins positively correlated with electrophysiological responses from AMPARs, 201 with $GABA_AR$s, and 113 with both. The collective of these proteins was found to be part of GO modules representing pre- and post-synapses, synaptic signaling, dendrite and mitochondrial structures, indicating its role in the sustenance of synaptic function. In addition, some of the proteins known to be associated with AMPAR or $GABA_AR$ post-synaptic density complexes [126,127]

positively correlated with MMSE scores and negatively with metrics of neuropathology (Figure 14) linking synaptic function and cognitive performance. We also observed a subset of 197 proteins that correlated positively with neuropathology severity and negatively with MMSE scores; 15% of these proteins also negatively correlated with the amplitude of AMPAR or $GABA_A$Rs (e. g. TJP1) suggesting a negative impact for synaptic function. Notably, the larger the amount of Aβ precursor protein (APP) and total tau in the synaptosomes the larger the *e*E/I ratio (Figure 14 b), and the larger the *e*E/I ratio the more variable and lower the MMSE scores (Figure 14 b). An unbiased hierarchical cluster analysis of all these data showed two major branches, one related with the sustenance of synaptic function and formed by proteins positively correlated with the electrophysiological function of synaptic receptors, lower neuropathology and better cognitive performance, and a second one related to synaptic toxicity, formed by proteins negatively correlated with synaptic receptor currents, with higher neuropathology and worse cognitive performance. Further GO analysis showed that 40 proteins common to all elements of the sustenance of synaptic function cluster are enriched in proteins related to mitochondrial matrix and complexes, and inorganic cation transmembrane transporter activity; and 30 proteins in the synaptic toxicity cluster are enriched in proteins related with nucleosome, cadherin binding and activation of innate immune response. Taken all together these results indicate that neuropathological changes and cognitive performance, as measured by MMSE, is a continuum, and alterations of the *e*E/I ratio have direct relationship with worsening of cognitive performance.

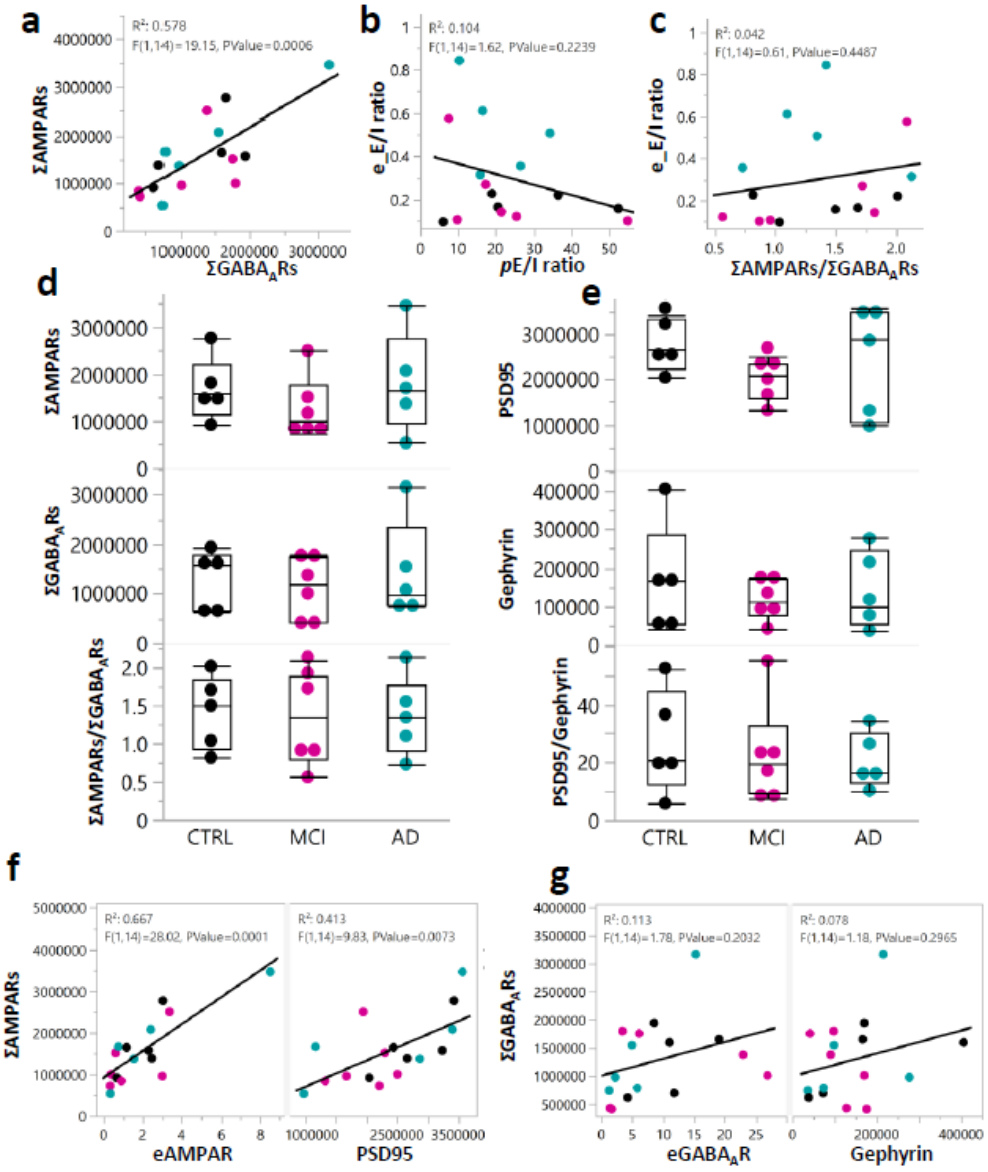

Figure 13 Proteomic analysis of excitatory and inhibitory synaptic receptors and markers. **a,** Sum of all AMPAR subunits (ΣAMPARs) and sum of all $GABA_AR$ subunits (Σ$GABA_ARs$) showed significant correlation (Pearson's correlation R^2 = 0.5776, p = 0.0006). **b, c,** No Correlation between the *e*E/I ratio with *p*E/I ratio (synaptic scaffold excitatory, PSD95; and inhibitory, GPHN) and with ΣAMPARs/ΣGABAARs. **d, e,** Synaptic receptors (AMPAR, $GABA_AR$) and synaptic markers (PSD95, GPHN) abundance and their ratios were similar within diagnostic groups. **f,** Notably, the abundance of AMPAR subunits correlated with the electrophysiological amplitude of AMPARs currents, **g,** but not for $GABA_AR$ subunits with the amplitude of $GABA_ARs$ responses or GPHN.

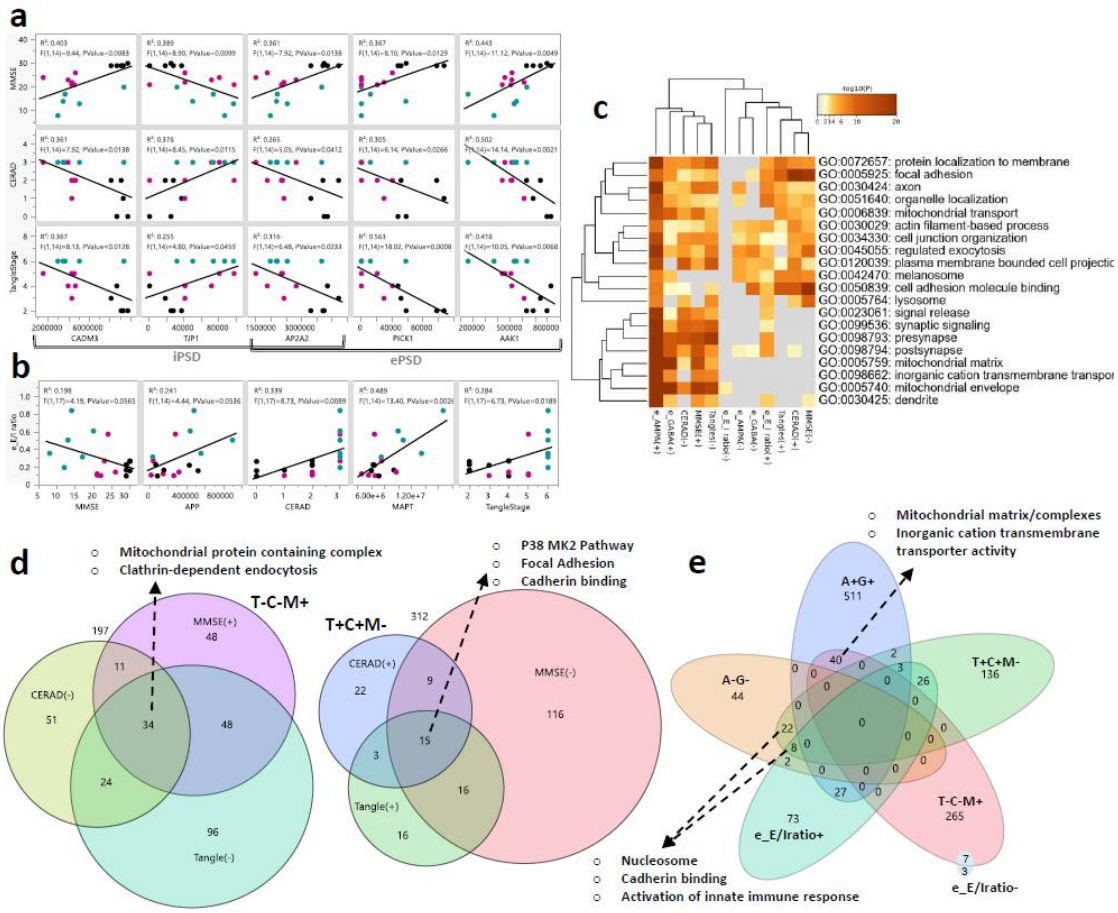

Figure 14 *e*E/I ratio correlates with severity of the pathology. a, Synaptic proteome profile reveals inhibitory and excitatory post-synaptic density proteins (iPSD, ePSD) correlating with MMSE and severity of AD pathology (Tangle score, CERAD) from CTRL (4+1pool), MCI (6) and AD (5) subjects. **b,** Pro-excitatory shift of the electrophysiological eE/I ratio associate with loss of cognitive performance and increase APP abundance, and strongly correlates with CERAD, tangles and tau levels. **c,** Metascape enrichment analysis of synaptic proteomic data correlating positively (+) or negatively (-) with MMSE (M), Tangle score (T), CERAD (C), eAMPA (A), eGABA (G), *e*E/I ratio (GO terms), spontaneously forms 2 separated clusters: AG+TC-M+ and AG-TC+M- *e*E/Iratio+, with *e*E/I ratio- not clearly included in one of the 2 clusters. **d,** Venn diagram showed 509 synaptic proteins correlating with at least one of the following variables: MMSE, tangles, and CERAD. Proteins correlating with MMSE(+)/Tangles(-)/CERAD(-) and MMSE(-)/Tangles(+)/CERAD(+) showed 2 independent clusters. Genes correlating with all the three variables from the left cluster are involved with mitochondrial processes and clathrin-dependent endocytosis; from the right cluster with P38 MK2 pathway, focal adhesion and cadherin binding. **e,** Venn diagram similarly as shown in **d,** but including eAMPA, eGABA and their ratio.

PRO-EXCITATORY SHIFT OF TRANSCRIPTIONAL SYNAPTIC EXCITATORY TO INHIBITORY RATIO IN ALZHEIMER'S DISEASE

We hypothesized that the imbalance of the synaptic E/I ratio in the TCx observed at the electrophysiological level in AD may be also observed at the mRNA level. Therefore, we used publicly available RNAseq dataset from the ADTBI study [128] to analyze the transcriptional E/I ratio (*t*E/I ratio) defined as the level of mRNA for PSD-95 (*DLG*4) over the level of mRNA for *GPHN* as we did for the PCx [129]. This analysis was done using hippocampi and TCx from non-demented controls with no pathology (n = 8) and AD subjects with tau pathology and abundant neuritic plaques (n = 12). Notably, in hippocampus and TCx the expression levels of inhibitory markers *GPHN* was significantly decreased (Figure 15 a) in AD subjects. On the contrary, expression levels of *DLG*4 in AD subjects were very similar to CTRL (Figure 15 a) in hippocampus and TCx. In both brain regions, the *t*E/I ratio showed a trend toward pro-excitatory changes in AD. To explore which genes had a potential effect on the *t*E/I ratio, we screened the whole gene expression dataset. We found more than 20 times more genes correlating with *t*E/I ratio in TCx compared with hippocampus (cutoff p = 0.001). In the TCx, 983 genes in CTRL and 1040 genes in AD were correlated with the *t*E/I ratio (Figure 15 b). Gene ontology analyses showed that those genes expressed proteins located at the postsynaptic region. Interestingly, genes related with *t*E/I ratio in AD were part of mRNAs codifying for proteins within, and adjacent to, the postsynaptic membrane: neurotransmitter receptors and the proteins that spatially and functionally organize them such as anchoring and scaffolding molecules. Hippocampus, showed only 36 genes for CTRL and 45 for AD correlated with the *t*E/I ratio, indicating a highly heterogenous and variable region across subjects. GO analysis was only possible to perform in AD. In CTRL, due the low number of correlated genes, the analysis did not find enrichment terms (Figure 15 b).

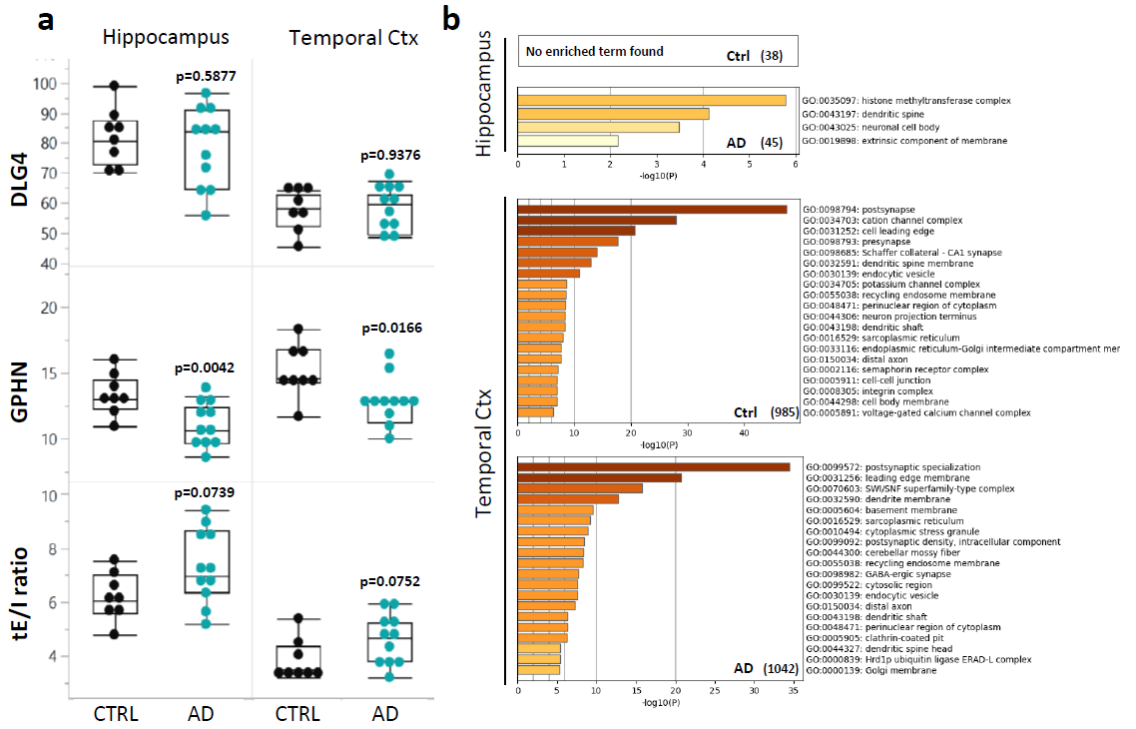

Figure 15. Transcriptomic reduction of inhibitory synaptic markers in AD, drives a shift of synaptic E/I balance toward a pro-excitatory trend. **a,** RNA-Seq datasets from the Aging, Dementia and Traumatic Brain Injury study (ADTBI) shows a differential alteration in gene expression of excitatory (*DLG4*) and inhibitory (*GPHN*) postsynaptic density proteins in hippocampus and TCx of CTRL and AD ($n = 8$ cognitive healthy controls, CERAD = 0 and 12 subjects with a DSM-IV clinical diagnosis of dementia of the AD disease type and AD pathology CERAD = 3). Levels of *GPHN* mRNA were significantly decreased in AD subjects, both in hippocampus (F (1, 18) = 10.95, p = 0.0042) and TCx (F (1, 18) = 7.06, p = 0.0166). No changes were found in *DLG4* expression levels in AD subjects in hippocampus (F (1, 18) = 0.006, p = 0.9376) and TCx (F (1,18) = 0.3054, p = 0.5877). In both brain regions, the *t*E/I ratio showed a trend toward pro-excitatory changes in AD (hippocampus: F (1, 18) = 3.63, p = 0.0739; TCX: F (1, 18) = 3.5909, p = 0.0752). Transcriptional synaptic *t*E/I ratio presents a trend of a shift toward pro-excitatory changes driven by the loss of inhibitory synaptic marker. **b,** Clusters of the gene ontology (GO) analysis reveals the cellular localization of genes positively correlated (threshold p = 0.001) with the *t*E/I ratio. TCx *t*E/I ratio correlates with genes expressed in the post-synaptic compartment in CTRL (985 genes) and AD (1042 genes). Hippocampus showed less genes correlating with *t*E/I balance (CTRL 38 genes; AD 45 genes). Response screening for CTRL was not sufficient powered to run the analysis due to the low number of genes. In AD, *t*E/I ratio was less representative of synaptic then TCx. Boxes extend from the 25th to 75th percentiles and the whiskers extend to 1.5*IQR (points behind the whiskers are considered outliers).

PRO-EXCITATORY SHIFT OF CELLULAR EXCITATORY TO INHIBITORY RATIO IN ALZHEIMER'S DISEASE

From the same Allen cohort, we used publicly available in situ hybridization image data from the ADTBI study [128], the numbers of glutamatergic neurons that expressed mRNA for the excitatory vesicular glutamate transporter 1 (vGluT1+$_{mRNA}$) and GABAergic neurons that expressed mRNA for GABA transporter 1 (GAT1+ $_{mRNA}$) were quantified for several subfields of hippocampus and TCx layers I-VI and (Figure 16 a). For these analyses, vGluT1+$_{mRNA}$ and GAT1+$_{mRNA}$ cells were counted in defined sample fields and their densities (number of cells/ area) compared between the AD and control groups. For measures of cellular E/I (*c*E/I) within hippocampus, several laminae were analyzed for either vGluT1+$_{mRNA}$ or GAT1+ $_{mRNA}$ cells and regional analyses were combined. Thus, excitatory vGluT1+ $_{mRNA}$ cells were counted in sample fields of CA3 stratum pyramidale and in the dentate hilar region referred to as CA4 , and inhibitory GAT1+$_{mRNA}$ cells were counted in CA3 stratum pyramidale, CA3 apical dendritic field, and the dentate gyrus molecular layer (Figure 16 a), and for each marker the counts across all sample fields were then averaged per case; this sampling strategy was used to access changes in the two cell types because inhibitory cells are more widely distributed across hippocampal subfields whereas excitatory cells are concentrated in specific laminae. Densities of vGluT1+ $_{mRNA}$ cells were not different between groups ($p = 0.4403$, two-tailed unpaired Student's t-test), whereas densities of GAT1+$_{mRNA}$ cells were significantly reduced in AD ($p = 0.0006$, two-tailed unpaired Student's *t*-test; Figure 16 b, C). Comparing the numbers of hippocampal vGluT1 to GAT1 expressing cells for each case demonstrated a marked increase in the cellular E/I ratio in the AD group ($p = 0.0087$, two-tailed unpaired Mann Whitney test; Figure 16 d-f). In TCx where both mRNAs were assessed within the same matched sample field (Figure 16 g), densities of vGluT1+ $_{mRNA}$ cells were not different between groups ($p = 0.2188$, two-tailed unpaired Student's *t*-test), whereas densities of GAT1+$_{mRNA}$ cells were significantly reduced in AD ($p = 0.0291$, two-tailed unpaired Student's t-test; Figure 16 h, i). Thus, like hippocampus, comparing the numbers of vGluT1 to GAT1 expressing cells in the cortical field for each case demonstrated a marked increase in the cellular E/I ratio in the AD group ($p = 0.007$, two-tailed unpaired Mann Whitney test; Figure 16 j, l). Overall,

these results support the conclusion that there are marked wide-spread decreases in GABAergic neurons that contribute to the increase in E/I ratio in AD brain.

PRO-EXCITATORY SHIFT OF CELLULAR AND TRANSCRIPTIONAL SYNAPTIC EXCITATORY TO INHIBITORY RATIOS IN ALZHEIMER'S DISEASE CORRELATES WITH LOSS OF COGNITIVE PERFORMANCE OF THE INDIVIDUALS

To corroborate our findings we test whether cellular and transcriptional synaptic E/I ratios calculated in the 8 CTRL and 12 AD individuals were correlated with cognitive impairment of the individuals as measured by the Cognitive Abilities Screening Instrument (CASI) which is based on Item Response Theory [35]. We decided to include also PCx in the analysis, that we previously studied[129], but we did not have cognitive scores of the subjects at the moment of the publication of the manuscript. In all the three brain regions (hippocampus, TCx, PCx), we observed that the higher the pro-excitatory shift of the *t*E/I and cE/I ratios were the more impaired the cognitive performance of the individuals was (Figure 17 a-f), especially memory. To avoid population bias effect, we also re-analyzed the *t*E/I ratio for 86 subjects available in the cohort from ACT study (demented individuals due to vascular, medical, multiple etiology or unknown causes were excluded). This data confirmed that the increase of the *t*E/I ratio in cortical areas is associated with loss of cognition (Figure 17 g-l). In contrast, in hippocampus the lower the inhibitory and excitatory synaptic markers levels the lower the cognitive score for that subject.

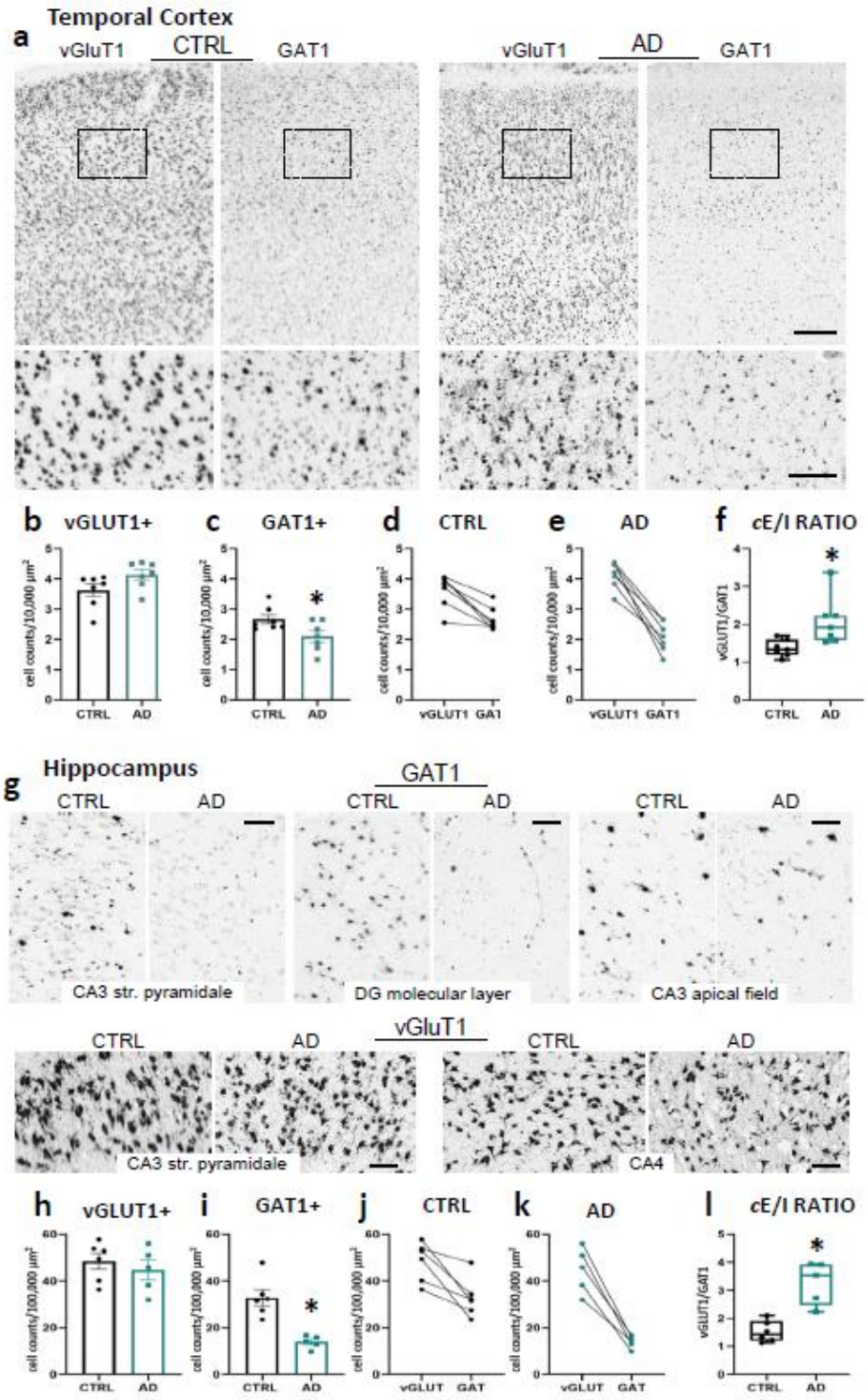

Figure 16. Marked reductions in GAT1 mRNA expressing cells in AD cases with dementia. **a,** Images showing in situ hybridization for vGluT1 and GAT1 mRNAs in TCx of a CTRL no dementia-CERAD 0 case and a dementia-CERAD 3 AD case. Box shows region that is presented at higher magnification (below). Calibration bars, 500 µm for top images; 200 µm for bottom images. **b, c,** Quantification of vGluT1 and GAT1 mRNA expressing cells in TCx per 100,000 μm^2. GAT1 expressing cells were reduced in the AD group (n = 7) versus the CTRL group (n = 7) (*p = 0.2188, two-tailed unpaired Student's t-test).

d-f, plots show the relative density of vGluT1 and GAT1 mRNA expressing cells for each CTRL **d,** and AD **e,** case, and the E/I ratio of the two measures for each case **f.** The cellular *c*E/I ratio in TCx was significantly elevated in the AD group versus CTRL (**p = 0.007, two-tailed unpaired Mann Whitney test). Data shown are based on a 30 μm^2 size threshold; separate analyses using 10 and 20 μm^2 size threshold yielded similar results. **g,** Images showing in situ hybridization for vGluT1 and GAT1 mRNAs in several hippocampal subfields targeted for analyses from CTRL no dementia-CERAD 0 and dementia-CERAD 3 AD cases. Calibration bars, 100 µm. **h, i,** Quantification of vGluT1 and GAT1 mRNA expressing cells per 100,000 μm^2. For vGluT1, measures from CA3 stratum pyramidale and CA4 were averaged, and for GAT1, measures from CA3 stratum pyramidale, CA3 apical dendritic field, and the dentate gyrus molecular layer were averaged (see Methods). GAT1 expressing cells were reduced in the AD group (n = 5) versus the CTRL group (n = 6) (***p = 0.0006, two-tailed unpaired Student's t-test). **j-l,** plots show the relative density of vGluT1 and GAT1 mRNA expressing cells for each control J. and AD **k,** case, and the E/I ratio of the two measures for each case **l,** The *c*E/I ratio in hippocampus was significantly elevated in the AD group versus controls (**p = 0.0087, two-tailed unpaired Mann Whitney test). In panels **f,** and **l,** blots show median values, 25th and 75th percentiles, and minimum and maximum range. In panels **b, c, h,** and **i,** whiskers represent standard errors.

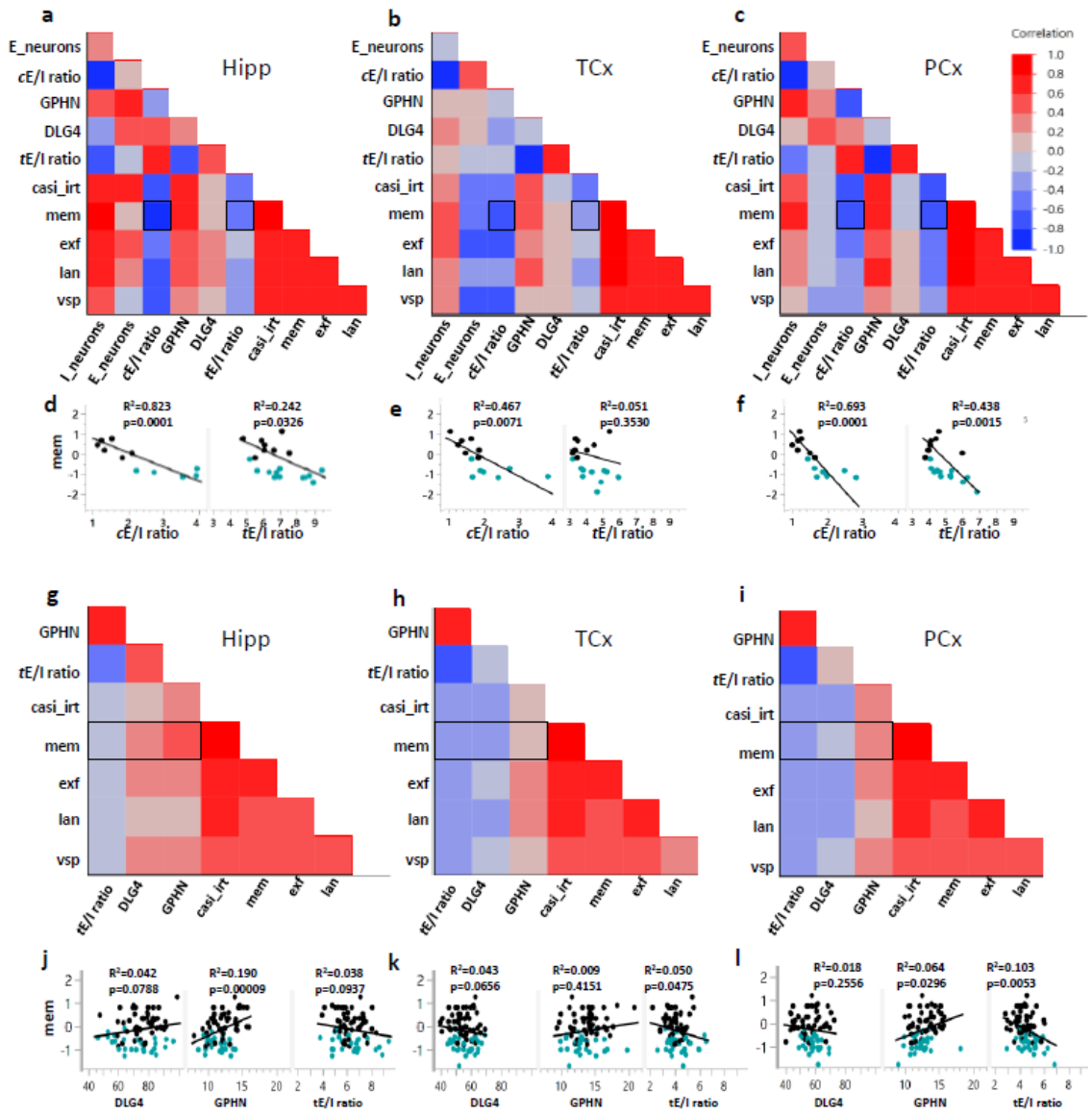

Figure 17. E/I balance in hippocampus, TCx, and PCx correlate with cognitive performance of the subjects. **a-c,** Multivariate analysis showing correlation maps for cognitive assessment scores of CTRL (8) and AD (12) subjects with cellular and synaptic excitatory markers, inhibitory markers, and their ratio (* = Pearson's correlation p-value < 0.05) from hippocampus, TCx and PCx. The subjects were scored with Cognitive Abilities Screening Instrument co-calibrated using item response theory (Casi_irt), memory (mem), executive function (exf), language (lan) and visual space (vsp). **d,** hippocampus, **e,** TCx and **f,** PCx showed cellular *c*E/I and *t*E/I ratios correlation with memory performance of the subjects (p values from Pearson's correlations). CTRL subjects are represented with black dots, AD with aqua dots. **g-i,** Pearson's correlation matrix showing cognitive assessments of 86 subjects (56 No demented, 30 demented AD's type), and RNA-seq data of synaptic excitatory (*DLG4*) and inhibitory (*GPHN*) markers and their ratio. **g,** Hippocampus (75), **h,** TCx (79) or **i,** PCx (74). **j,** In hippocampus, memory loss showed significative correlation with reduction of inhibitory synaptic markers, and a trend with loss of excitatory synaptic markers. **k, l,** Cortical regions showed that memory loss better correlates with *t*E/I ratios increase.

CHAPTER 3. METHODS

Increased functional Excitatory to Inhibitory synaptic ratio in parietal cortex of Alzheimer's disease subjects

CASES AND TISSUE SAMPLES.

AD and DS PCx tissue was provided by the UCI Institute for Memory Impairments and Neurological Disorders through the UCI-Alzheimer's Disease Research Center (ADRC). Control tissue was provided by the NINDS/NIMH sponsored Human Brain and Spinal Fluid Resource Center at the VA West Los Angeles Healthcare Center, Los Angeles, CA. All cases were de-identified and coded by the source tissue banks. For the present studies, the samples were recoded and processed for all analyses with the experimenter blind to subject and group. The study was reviewed by the Institutional Review Boards of the University of California at Irvine and the University of Texas Medical Branch and categorized as a non-human subject study.

Postmortem human PCx tissue blocks, that included a well-defined sulcus with portions of gyri present on both sides, were obtained from 5 controls, 5 AD cases and 6 DS cases, with both males and females included in the analyses. While effort was made to match age and postmortem interval (PMI) as closely as possible, the control group contained longer PMIs; in preliminary studies PMIs up to ~25 h did not significantly affect FDT- or MSM- based synapse measures, consistent with earlier work [100] and with our study evaluating the effects of postmortem interval on synaptic metrics. All DS and AD cases underwent formal neuropathological evaluation in the ADRC Neuropathology Core and demonstrated Braak stage VI neurofibrillary degeneration [130] and Consortium to Establish a Registry for Alzheimer's Disease (CERAD) as frequent in cerebral cortex neuritic plaque density [19]. Functional levels of independence were comparable between the two groups as determined by the modified version of the Bristol Activities of Daily Living Scale (mBADLS) that was collected within the last 1-2 years of life [131] . In addition, in a recent

study Western blotting and antibodies to AT8 were used to assess the levels of hyperphosphorylated (p)-tau in tissue sections obtained from the same tissue blocks used here [132]. Those data are presented here again for each sample in order to directly compare a hallmark of AD pathology with measures of excitation and inhibition for each case.

For both FDT and MSM analyses, each fresh-frozen tissue block was cut on a cryostat at 20 µm perpendicular to the tissue surface and sections were collected. For FDT, sections were slide-mounted, methanol-fixed, and stored at -20°C prior to processing for double-labeling immunofluorescence. For MSM analyses, a single tissue section was collected into a microcentrifuge tube and stored at -80°C until processed as described below.

DIAGNOSIS	N	AGE	SEX	PMI (H)	AD PATHOLOGY	M-BADLS
CONTROL	5	57.2 ± 4.9	4M/1F	15.4 ± 4*		
AD	5	57.8 ± 2.2	2M/3F	3.8 ± 1	Stages VI/C	27.4 ± 13.7
DS	6	56.3 ± 3.5	3M/3F	4.1 ± 1	Stages VI/C	33.2 ± 9.3

Table 1. Summary of demographics, pathology, and cognitive skills for study groups. Values for age, postmortem interval (PMI), and the modified version of the Bristol Activities of Daily Living Scale (mBADLS) are mean ± SD. ANOVA test showed significant difference (*) of PMI of CTRL compared to the two pathological groups ($p < 0.05$). See text for further details. Copied with permission from[129].

FLUORESCENCE DECONVOLUTION TOMOGRAPHY

Tissue sections were processed for double-labeling immunofluorescence as described [133], using antisera directed against the excitatory synapse scaffold protein PSD-95 to label excitatory synapse postsynaptic densities (PSDs) [134] in combination with

antisera directed against the inhibitory synaptic marker GPHN as previously described [135,136]. Antibodies used were mouse anti-PSD-95 (1:1000; Thermo Scientific, #MA1-045) and rabbit anti-GPHN (1:1000; Abcam, ab32206), with species-specific Alexafluor488 and Alexafluor594 conjugated secondary antibodies (1:1000 each; Thermo Fisher Scientific) for visualization. For FDT, image z-stacks of layer 1 and layer 2 PCx were collected using a 1.4 NA 63X objective through a depth of 2 μm with 0.2 μm steps using a Leica DM6000 epifluorescence microscope equipped with a Hamamatsu ORCA-ER digital camera; the sample field size for each cortical layer measured 42,840 μm^3. Both layers 1 and 2 were assessed for analyses because depth placement of the sample field, relative to the cortical surface, could be reliably replicated, and to compare a relatively cell sparse versus cell dense layer. Numbers of immunolabeled synapses in the two layers ranged from 25,000-30,000 per stack. For each layer, 10-12 image stacks from three sections per brain were taken from within the sulcus of each sample, and then processed for iterative deconvolution using Volocity 4.1 (Perkin Elmer). Deconvolved images were analyzed using in-house software to quantify all labeled puncta within the size constraints of synapses as previously described [133,135–137]. Background staining variations in the deconvolved images were normalized to 30% of maximum background intensity using a Gaussian filter, and object recognition and measurements of immunolabeled puncta were automated using in-house software built using Matlab R2007, Perl, and C that allows for detailed analysis of objects reconstructed in 3D. Pixel values (8-bit) for each image were multiply binarized using a fixed-interval intensity threshold series followed by erosion and dilation filtering to reliably detect edges of both faintly and densely labeled structures. Object area and eccentricity criteria were then applied to eliminate elements, including lipofuscin granules, that do not fit the size and shape range of synaptic structures from the quantification. Counts of immunolabeled objects were averaged across sections to produce mean values per subject. Statistical comparisons to identify the effect of group used a one-way ANOVA followed by Newman-Keuls Multiple Comparison test for post-hoc paired comparisons (GraphPad Prism, Version 5.0). If variances across groups were not equal, as determined by Bartlett's test, then the Welch ANOVA or nonparametric Kruskal-Wallis test was used followed by Dunn's Multiple Comparison test. In other comparisons, repeated-measures ANOVA was used followed by Student Newman Keuls post-hoc test. In all cases, $p < 0.05$ was

considered significant. Pearson product-moment was used for all the linear correlations using JMP version 14 (SAS Institute, Cary, NC).

MICROTRANSPLANTATION OF SYNAPTIC MEMBRANES AND FLOW CYTOMETRY.

Membrane preparations were isolated from a single 20 µm slice of frozen PCx from each brain donor using Syn-PER method (Thermo Fisher Scientific); on average, the tissue blocks ranged in size from ~25-35 mm (length) by 15-20 mm (width). Briefly, a tissue slice was placed in an Eppendorf tube and stored at -70º C until processed. To make synaptic membranes, each slice was suspended in 500 µl of Syn-PER extraction reagent, transferred to 2 mL glass/Teflon Dounce and stroked slowly for 15 times. The homogenate was then transferred to 1.5 mL Eppendorf and centrifuged at 1200 g (4° C) for 10 min. The supernatant (S1) was transferred to a new Eppendorf and centrifuged at 15,000 g for 20 min. The pellet enriched in synaptosomes (P2) was resuspended in 15 µL of Syn-Per solution, aliquoted and stored at -80° C until further use for electrophysiology experiments. The amount of protein was determined using the Qubit protein assay reagent kit (Thermo Fisher Scientific). Numbers of particles within the size of synaptosomes were counted as described previously [138–140], using appropriate size standards (Spherotech, Inc), in a Guava EasyCyte flow cytometer (EMD Millipore) and analyzed using Incyte software (EMD Millipore). Synaptosomes were sonicated in iced-water 3 times for 5 seconds, at 1 min intervals between sonications, to create small proteoliposomes that can fuse to the oocytes' extracellular membrane. One day before electrophysiological recordings the synaptic membranes were injected into stage V-VI *Xenopus laevis* oocytes using protocols previously published for cellular membranes[83,100,141]. Each oocyte was injected with 50 nL of synaptic proteoliposomes (2 mg/mL protein concentration).

ELECTROPHYSIOLOGICAL RECORDINGS

Ion currents elicited by agonist perfusion were recorded by the two-electrode voltage clamp (TEVC) method between 18-36 h post injection [83]. Microelectrodes were filled with 3 M KCl and resistance of the microelectrodes ranged from 0.5–3.0 MΩ. Piercing and recording took place in a chamber (volume ≈0.1 ml) continuously perfused (6 ml/min) with Ringer's solution [115 mM NaCl, 2 mM KCl, 1.8 mM $CaCl_2$, 5 mM Hepes (pH 7.4)] at room temperature (19–21°C). Oocytes were voltage clamped to −80 mV. Ion currents were recorded and stored with WinEDR ver 2.3.8 Strathclyde Electrophysiology Software (John Dempster, Glasgow, United Kingdom). Kainic acid, s-AMPA were purchased from Tocris (Minneapolis, MN). All other reagents were from Sigma (St. Louis. MO). Working solutions were made by diluting stock solutions in Ringer's solution. A total of 7 frogs were used for MSM experiments. For all measures, for each subject, electrophysiological recordings were done at least in triplicate (three oocytes) in batches of oocytes from 2-4 different frogs, balancing the groups for equal number of subjects in each experimental run. Statistical comparisons to identify the effect of diagnosis used the mean of each metric, for each subject, as experimental unit in a one-way ANOVA, followed by post-hoc Dunnett's multiple comparisons versus control test (JMP, version 14). If variances across groups were not equal, then the Welch ANOVA or nonparametric Kruskal-Wallis test was used followed by Dunn's comparison vs control test. As a matter of confirmation, we also implemented a nested ANOVA with random effects mixed model, wherein the subjects were nested within diagnosis, and subject was tested as a random effect using the expected mean squares method. In all cases, $p < 0.05$ was considered significant. Pearson product-moment was used for linear correlations, and Spearman's rank for non-parametric correlations, using JMP version 14.

Neuronal, synaptic and electrophysiological Excitatory to Inhibitory imbalance associates with loss of cognitive performances in Alzheimer's Disease individuals

HUMAN TISSUE

The UCI Institute for Memory Impairments and Neurological Disorders through the UCI-Alzheimer's Disease Research Center (ADRC) provided hippocampi and medial temporal cortices from CTRL, MCI and AD subjects. All cases were de-identified and coded by the source tissue banks. For the present studies, the samples were recoded and processed for all analyses with the experimenter blind to subject and group. The study was reviewed by the Institutional Review Boards of the University of California at Irvine and the University of Texas Medical Branch and categorized as a non-human subject study. All brains were processed within a post-mortem interval (PMI) of 6.17 h.

OOCYTES EXTRACTION AND ISOLATION

Oocytes from *Xenopus Laevis* were used to perform MSM as previously reported [125,129]. Frogs were anesthetized in a bath containing 0.17% tricaine for 10–15 min before extracting the ovaries; following procedures in accordance with the National Institutes of Health Guide for the Care and Use of Laboratory Animals at the University of Texas Medical Branch at Galveston (IACUC:1803024). To remove the follicular layer, oocytes were incubated for 4.5h at 31°C with 0.2% collagenase type I in Barth's solution [88 mM NaCl, 1 mM KCl, 0.41 mM $CaCl_2$, 0.82 mM $MgSO_4$, 2.4 mM $NaHCO_3$, 5 mM HEPES (pH 7.4)]. Finally, the oocytes were washed using Barth's solution. Healthy spherical oocytes with no signs of tear, and developmental stages V-VI, were selected for MSM experiments.

SYNAPTOSOMAL FRACTION (P2) PREPARATION

Described in Chapter 3 "Microtransplantation of synaptic membranes and flow cytometry"

P2 IMMUNOSTAINING AND FLOW CYTOMETRY

P2 fraction pools for each group and brain region were removed from -80°C freezer and gradually thawed in ice for 20 min. Then, 1 µL of the P2 fraction was transferred in a new Eppendorf tube containing 200 µL of 4 % paraformaldehyde pH 7.4 (PFA) and incubated for 1h at 4°C. Within the incubation, after 30 min, the samples were gently mixed by pipetting up and down 3 times and replaced at 4°C for the remaining 30min. PBS (400 µL) (Thermo scientific cat#TA125PB) was added and the samples were centrifuged for 8 min at 5000 g to pellet the P2 fraction. The P2 fraction was resuspended in 150 µl permeabilization buffer (PBS + Tween20 0.3%), incubated 20 min at 32°C and centrifuged 8min at 5000g. The supernatant was discarded and the pellet was resuspended with 40µL of blocking solution (PBS + FBS 2%) and incubated with post-synaptic antibody overnight. Anti-PSD-95(1:80, Novus-NB300-556AF647) or Anti-GPHN (1:100, Abcam-Ab32206) were used to label post-synaptic densities. GPHN required an additional 1h incubation with secondary antibody (1:400, Invitrogen-A11008). After washing with PBS to eliminate no-specific binding, flow cytometry analysis was performed on P2 fractions using Guava 3.3 soft. and Guava EasyCyte flow cytometer (EMD Millipore). A size gate based on forward and side scatters were built using size beads (Spherotech Inc.). P2 samples were diluted 1:500 in PBS and then loaded into the flow cytometer. The instrument was set to count 5000 events within the main gate. To each particle within the synaptosome gate was assigned a value of fluorescence intensity: red (PSD-95) or green (GPHN) fluorescence.

MICROTRANSPLANTATION OF SYNAPTIC MEMBRANES

MSM was performed as described in Chapter 3, "microtransplantation of synaptic membranes and flow cytometry"

TRANSCRIPTOME ANALYSIS

To estimate the transcriptional E/I (tE/I) ratio in hippocampus and TCx, publicly available RNA-seq data from ADTBI study were analyzed [27]. The dataset was downloaded from the website (http://aging.brain-map.org/download/index). Analysis was restricted to 20 subjects that matched Control and AD parameters based on manual of mental disorders IV (DSM-IV) and CERAD score. Eight cognitively intact subjects (no dementia, CERAD = 0), 5 males and 3 females age included between 78 and 100 years old; and 12 demented AD-type subjects showed neuropathological hallmarks of AD (DSM-IV clinical diagnosis Alzheimer's disease and CERAD = 3), 6 males and 6 females age matched with the control group. We analyzed transcriptome from hippocampus and TCx of 20 subjects (8 CTRL and 12 AD). The tE/I ratio for each subject was calculated based on their ratio of the fragments per kilobase of transcript per mapped (FPKM) reads for PSD-95 transcript *DLG*4 to *GPHN* mRNA, and then the effects of age, sex, and PMI on this measure. The RNA-seq dataset was screened to find genes correlating with *DLG*4/GHPN ratio (cut-off = 0.001). Gene Ontology analysis was performed on those genes to find their cellular localization.

IN SITU HYBRIDIZATION ANALYSES

Full-size, high-resolution images of colorimetric in situ hybridization (ISH) for vGluT1 (SLC17A7) and GAT1 (SLC6A1) mRNA expressing cells in TCx and hippocampus were downloaded from ADTBI study website (http://aging.brain-map.org/donors/summary). For both brain areas, cases assessed were a subgroup of those used for the gene expression analyses because not all the cases have both, RNAseq and ISH data; additionally, AD case H14.09.042 did not have TCx images, and AD case H14.09.098 did not have hippocampal images. For TCx, 7 control and 7 AD cases were analyzed. For each case, the TCx vGluT1 and GAT1 images were cropped to the same size sample field (e.g., 9,000,000 um2) to encompass all layers 1-VI of the cortical field; the location of each sample field was matched between the images for each mRNA. Three cropped images for each mRNA was assessed per case with the mean total area assessed for the control and AD groups being 34,920,000 ± 2,545,480 μm2 and 34,191,429 ±

3,603,269 μm2, respectively (p = 0.669). Automated counts of labeled TCx cells were performed using scikit-image 0.16.2 and Python 3.7 as previously described [129]. Images were Gaussian blurred at 3 pixel sigma to remove small imaging artifacts and then thresholded using a Yen intensity threshold [129], which was found to be optimal across numerous thresholding methods blind-tested across several images. Cell objects were counted at multiple thresholds (10, 20, and 30 pixels) and while all yielded similar differences in E/I ratios between groups, the larger 30 um^2 size threshold size was chosen for final analyses. Values were expressed per 100,000 μm^2.

For hippocampus which has well defined anatomical subfields, 6 control and 5 AD cases were selected for analyses using the criteria that each case had to have a visible dentate gyrus, region CA4 and CA3; this resulted in the exclusion of 1 control, and 3 AD cases with poorly defined regions. Since region CA1 was not present in all of the final cases this field was excluded from analyses. Unlike cortex, where excitatory and inhibitory cells are interspersed across the cortical layers, hippocampal excitatory cells are localized within specific lamina (e.g., stratum pyramidale and, in human, within the dentate hilar region referred to as CA4). Inhibitory cells are distributed throughout the hippocampus but also exclusively in the molecular layers which are devoid of excitatory neurons (e.g., CA3 apical dendritic field, and the dentate gyrus molecular layer). Thus, for relative E/I ratios in hippocampus, vGluT1 mRNA positive cells were counted in sample fields of both CA3 stratum pyramidale and CA4, and GAT1 mRNA positive cells were counted in sample fields of CA3 stratum pyramidale, CA3 apical dendritic field, and the dentate gyrus molecular layer. For each mRNA, three cropped images were obtained per sample field for each case. The mean size of each sample field was: CA3 stratum pyramidale, 450,000 μm2 (the location of the sample field was matched between the images for both mRNAs); CA4, 600,000 μm2; CA3 apical dendritic field, 320,000 μm2; dentate gyrus molecular layer, 500,000 μm2. Automated counts of GAT1 labeled cells were performed as described above, and objects were counted if they were larger than 30 pixels. Because the vGluT1 labeled cells in the hippocampal fields were more greatly packed together and often touched other label cells, these cells were counted manually using the same size criteria to avoid potential confounds that would occur with automated counting. Images were imported into ImageJ, and cells were counted using the multi-point tool by three

independent scorers blind to cases and groups. The three scores for each image were then averaged for a final cell count for each vGluT1 image field. For final vGluT1 and GAT1 counts, numbers were averaged across all sample fields for each mRNA and values of labeled cells were expressed per 100,000 μm^2. Either two-tailed unpaired Student's t-test or a two-tailed unpaired Mann Whitney test were used for statistical analyses between the two groups and were conducted using Prism 9.1.1.

PROTEOMIC ANALYSIS USING NANOFLOW LIQUID CHROMATOGRAPHY-TANDEM MASS SPECTROMETRY

P2 fractions (2µg/µL) were sonicated 6 times for 5s as we use for MSM, then 1µL were analyzed by nanoflow liquid chromatography-tandem mass spectrometry (nanoLC-MS/MS) using a nano-LC chromatography system (UltiMate 3000 RSLCnano, Dionex, Thermo Fisher Scientific, San Jose, CA). The nanoLC-MS/MS system was coupled on-line to a Thermo Orbitrap Fusion mass spectrometer (Thermo Fisher Scientific, San Jose, CA) through a nanospray ion source (Thermo Scientific). A trap and elute method was used to desalt and concentrate the sample, while preserving the analytical column. The trap column (Thermo Scientific) was a C18 PepMap100 (300um X 5mm, 5um particle size) while the analytical column was an Acclaim PepMap 100 (75µm X 25 cm)(Thermo Scientific). After equilibrating the column in 98% solvent A (0.1% formic acid in water) and 2% solvent B (0.1% formic acid in acetonitrile (ACN)), the samples (2 µL in solvent A) were injected onto the trap column and subsequently eluted (300 nL/min) by gradient elution onto the C18 column as follows: isocratic at 2% B, 0-5 min; 2% to 28% B, 5-120 min; 28% to 40% B, 120-124 min; 40% to 90% B, 124-126 min; isocratic at 90% B, 126-130 min; 90% to 2%, 130-132 min; and isocratic at 2% B, until the 150 minute mark. All LC-MS/MS data were acquired using XCalibur, version 2.4.0 (Thermo Fisher Scientific) in positive ion mode using a top speed data-dependent acquisition (DDA) method with a 3 second cycle time. The survey scans (m/z 350-1500) were acquired in the Orbitrap at 120,000 resolution (at m/z = 400) in profile mode, with a maximum injection time of 100 msecond and an AGC target of 400,000 ions. The S-lens RF level was set to 60. Isolation was performed in the quadrupole with a 1.6 Da isolation window, and CID MS/MS

acquisition was performed in profile mode using rapid scan rate with detection in the ion-trap using the following settings: parent threshold = 5,000; collision energy = 32%; maximum injection time 56 msec; AGC target 500,000 ions. Monoisotopic precursor selection (MIPS) and charge state filtering were on, with charge states 2-6 included. Dynamic exclusion was used to remove selected precursor ions, with a +/- 10 ppm mass tolerance, for 15 seconds after acquisition of one MS/MS spectrum. Tandem mass spectra were extracted and charge state deconvoluted using Proteome Discoverer (Thermo Fisher, version 2.2.0388). Deisotoping was not performed. All MS/MS spectra were searched against a Uniprot Homo Sapiens protein FASTA database using Sequest. Searches were performed with a parent ion tolerance of 5 ppm and a fragment ion tolerance of 0.60 Da. Trypsin is specified as the enzyme, allowing for two missed cleavages. Fixed modification of carbamidomethyl (C) and variable modifications of oxidation (M) and deamidation were specified in Sequest.

CHAPTER 4. CONCLUSION

Aberrant hyperactivation of specific brain regions occurs already in prodromal AD, and its correction may have disease-modifying effects. Growing evidence associate AD hyperactivation with E/I imbalance at the level of the synapses[142]; high synaptic activity induces perisynaptically release of tau and Aβ proteins [95,143,144], and high levels of those proteins increase synaptic activity [53,55] suggesting a self-feeding loop with deleterious consequences for neuronal function. In addition, global synaptic E/I ratio positively correlates with neuronal firing [145], suggesting that hyperactive brain regions may have a shift of the E/I ratio toward pro-excitatory changes.

Using multiple orthogonal approaches, three independent cohorts and three brain regions, we report here evidence of E/I imbalance in the AD brain that favors greater synaptic excitation in areas found to be hyperactive in AD using fMRI. Using near-simultaneous recording of synaptic receptors (AMPAR and $GABA_AR$), we reported a pro-excitatory shift of E/I balance in TCx and PCx of AD subjects. Because AD is a continuum, TCx pro-excitatory *e*E/I ratio correlates with higher levels of AD biomarkers and strongly associated with impairment of the cognition of the subject. In hippocampus, the lower the amplitude of synaptic currents was the lower the mental score of the subject, suggesting an equal and parallel deterioration of the excitation and inhibition. To corroborate those findings, we used an independent cohort using RNA-seq and hibridization in situ dataset available online to estimate transcriptional synaptic (*t*E/I) and cellular (cE/I) E/I ratio. The cE/I ratios in all three brain regions were strongly correlated with the memory score of the subjects: the more pro-excitatory the shift was the more impairment in memory. Same outcome was observed with *t*E/I ratios. PCx and hippocampus showed a correlation in the same direction, but not TCx. While our results showed E/I imbalance in AD, whether this phenomenon comes before toxic oligomers productions still not known. The robust pro-excitatory shift

of E/I balance associated with loss of cognition and pathology severity suggest that there is a strong connection between these events.

We cannot exclude the possibility that these synaptic E/I effects might reflect a feature of early-onset AD such as seizure activity [146,147], however, complementary findings from the ADTBI cohort suggest that E/I imbalance is not an exclusive feature of early-onset AD. In particular, gene expression analyses for both PSD-95 and *GPHN* transcripts and vGluT1 and GAT1 expressing cells in the ADTBI cohort of subjects, with late-onset AD and level of pathology similar to the ones used in FTD studies, also demonstrated a shift in E/I imbalance. Electrophysiological recordings from the MSM studies also showed unequal deficits in postsynaptic AMPAR- and $GABA_AR$ mediated ion currents, leading to an increase in the global electrophysiological synaptic E/I ratio in cortical areas but not in hippocampus, which would favor enhanced synaptic excitatory drive. The E/I shift in AD is remarkable in the context of studies showing that synaptic levels of inhibition are generally proportional and scaled in strength to excitation, despite even large variations in the amplitude of excitatory synaptic currents across neurons [81,88,110]. Changes in excitatory synapse number and/or strength predicted for Hebbian plasticity during learning and memory are similarly compensated for by synaptic scaling [111], heterosynaptic plasticity [110], and changes in synaptic function within minutes and hours[112]. Indeed, the E/I ratio in our MSM study had minimal variation compared to ion currents measured individually, indicating that on average the relationship between postsynaptic AMPARs and $GABA_ARs$ is nearly constant in control individuals. While our results do not identify the cell types receiving higher excitatory drive in AD, the large majority of neurons in cortex are excitatory pyramidal cells [148], suggesting that these are the principal target. Consistent with this, there is enhanced excitatory transmission in principal neurons due to GABAergic deficits in animal models of familial AD [52,149,150]. Interneurons are somewhat protected compared to pyramidal neurons in AD at early stages, but nonetheless exhibit morphological alterations and innervation deficits [151], particularly adjacent to amyloid

pathology [152], that are likely to underlie the beginning of synaptic inhibitory dysfunction in the disorder. Based on our gene expression findings for advanced AD, we propose that as the disease progresses there are more cell-wide effects on inhibitory neurons, which would be expected to further exaggerate E/I deficits. The cellular mechanisms contributing to the emergence and progression of AD are poorly understood. Multiple studies have described dysfunctions in cholinergic and glutamatergic systems [153,154]but it is not known if equivalent disturbances occur in the GABA system. Post-mortem AD studies of GABA levels, or the distribution or activity of the GABA synthesizing enzyme glutamic acid decarboxylase (GAD), have obtained mixed results, with reports indicating reductions or no change in GABA or GAD levels (see [155] for a comprehensive review). Analyses of $GABA_A$Rs in the AD brain have reported decreases in protein levels for the α1, α5, β3, and γ2 subunits [155], and preservation or up-regulation of subunits that are normally co-expressed in the human brain [124,155]. Total levels of GPHN immunoreactivity are reported to decrease with increasing pathology in the AD brain [105] and there is evidence for a transcriptional decoupling between $GABA_A$R subunits and *GPHN*, two effects that would be consistent with inhibitory deficits in AD. Of interest in this regard is evidence that GPHN becomes abnormally associated with Aβ plaques and occasionally with NFTs [107]. However, no studies to date have evaluated synaptic levels of GPHN in AD. Thus, the present findings demonstrating that the density of GPHN-ir in synapse-size puncta is more greatly reduced than those for PSD-95-ir in AD PCx indicates a relatively greater deficit at inhibitory synapses and thus an increase in "uncompensated" excitatory connectivity.

In conclusion, anatomical, electrophysiological, cellular and transcriptional data indicate that dysregulation of the inhibitory system drives a pro-excitatory shift of synaptic E/I ratio. Imbalance of this ratio seems to be responsible of the hyperactivity of TCx and PCx, and strongly correlates with cognitive loss. Anti-epileptic drug has proven to be beneficial to AD subjects, even though more specific targets are required to produce efficient therapies. This evidence opens to the possibility of new potential therapies direct

to the correction of GABAergic system in specific regions hyperactive in AD, as TCx and PCx to restore the physiological E/I ratio, and more important restore the cognition of the subjects.

CHAPTER 5. REFERENCES

1. DeTure, M. A. & Dickson, D. W. The neuropathological diagnosis of Alzheimer's disease. *Mol. Neurodegener.* **14**, (2019).
2. A, Chandra, G, Dervenoulas, M, Politis. Magnetic resonance imaging in Alzheimer's disease and mild cognitive impairment. *J. Neurol.* **266**, 1293–1302 (2019).
3. Nelson, P. T., Braak, H. & Markesbery, W. R. Neuropathology and Cognitive Impairment in Alzheimer Disease: A Complex but Coherent Relationship. *J. Neuropathol. Exp. Neurol.* **68**, 1–14 (2009).
4. Kamenetz, F. *et al.* APP processing and synaptic function. *Neuron* **37**, 925–37 (2003).
5. Pearson, H. A. & Peers, C. Physiological roles for amyloid beta peptides. *J. Physiol.* **575**, 5–10 (2006).
6. Avila, J., Lucas, J. J., Pérez, M. & Hernández, F. Role of Tau Protein in Both Physiological and Pathological Conditions. *https://doi.org/10.1152/physrev.00024.2003* **84**, 361–384 (2004).
7. Guo, T., Noble, W. & Hanger, D. P. Roles of tau protein in health and disease. *Acta Neuropathologica* **133**, 665–704 (2017).
8. Serrano-Pozo, A., Frosch, M. P., Masliah, E. & Hyman, B. T. Neuropathological alterations in Alzheimer disease. *Cold Spring Harb. Perspect. Med.* **1**, a006189 (2011).
9. Chen, M.-K. *et al.* Assessing Synaptic Density in Alzheimer Disease With

Synaptic Vesicle Glycoprotein 2A Positron Emission Tomographic Imaging. *JAMA Neurol.* **75**, 1215 (2018).

10. 2020 Alzheimer's disease facts and figures. *Alzheimer's Dement.* **16**, 391–460 (2020).
11. Mehta, D., Jackson, R., Paul, G., Shi, J. & Sabbagh, M. Why do trials for Alzheimer's disease drugs keep failing? A discontinued drug perspective for 2010-2015. *Expert Opin. Investig. Drugs* **26**, 735–739 (2017).
12. DS, Knopman, DT, Jones, MD, Greicius. Failure to demonstrate efficacy of aducanumab: An analysis of the EMERGE and ENGAGE trials as reported by Biogen, December 2019. *Alzheimers. Dement.* **17**, 696–701 (2021).
13. Hippius, H. & Neundörfer, G. The discovery of Alzheimer's disease. *Dialogues Clin. Neurosci.* **5**, 101–8 (2003).
14. McKhann, G. *et al.* Clinical diagnosis of Alzheimer's disease: report of the NINCDS-ADRDA Work Group under the auspices of Department of Health and Human Services Task Force on Alzheimer's Disease. *Neurology* **34**, 939–44 (1984).
15. Perl, D. P. Neuropathology of Alzheimer's disease. *Mt. Sinai J. Med.* **77**, 32–42 (2010).
16. McKhann, G. M. *et al.* The diagnosis of dementia due to Alzheimer's disease: recommendations from the National Institute on Aging-Alzheimer's Association workgroups on diagnostic guidelines for Alzheimer's disease. *Alzheimers. Dement.* **7**, 263–9 (2011).
17. How Is Alzheimer's Disease Diagnosed? *NIH, 2019* Available at:

https://www.nia.nih.gov/health/how-alzheimers-disease-diagnosed. (Accessed: 23rd September 2019)

18. Braak, H. & Braak, E. *Neuropathological stageing of Alzheimer-related changes*. *Acta Neuropathol* **82**, (1991).

19. Mirra, S. S. *et al.* The consortium to establish a registry for Alzheimer's disease (CERAD). Part II. Standardization of the neuropathologic assessment of Alzheimer's disease. *Neurology* **41**, 479–486 (1991).

20. DA, B. *et al.* Neuropathology of older persons without cognitive impairment from two community-based studies. *Neurology* **66**, 1837–1844 (2006).

21. Meraz-Ríos, M. A., Toral-Rios, D., Franco-Bocanegra, D., Villeda-Hernández, J. & Campos-Peña, V. Inflammatory process in Alzheimer's Disease. *Front. Integr. Neurosci.* **7**, 59 (2013).

22. Alzheimer's Facts and Figures Report | Alzheimer's Association. Available at: https://www.alz.org/alzheimers-dementia/facts-figures. (Accessed: 3rd September 2019)

23. Reitz, C. & Mayeux, R. Alzheimer disease: epidemiology, diagnostic criteria, risk factors and biomarkers. *Biochem. Pharmacol.* **88**, 640–51 (2014).

24. Dong, H. K., Gim, J.-A., Yeo, S. H. & Kim, H.-S. Integrated late onset Alzheimer's disease (LOAD) susceptibility genes: Cholesterol metabolism and trafficking perspectives. *Gene* **597**, 10–16 (2017).

25. Bekris, L. M., Yu, C.-E., Bird, T. D. & Tsuang, D. W. Genetics of Alzheimer disease. *J. Geriatr. Psychiatry Neurol.* **23**, 213–27 (2010).

26. Potter, H., Granic, A. & Caneus, J. Role of Trisomy 21 Mosaicism in Sporadic and

Familial Alzheimer's Disease. *Curr. Alzheimer Res.* **13**, 7–17 (2016).

27. Blennow, K., De Leon, M. J. & Zetterberg, H. *Alzheimer's disease*. Lancet (London, England), **368**, 9533, 7 (2006).

28. Cummings, J. L. Alzheimer's Disease. *N. Engl. J. Med.* **351**, 56–67 (2004).

29. Silva, M. V. F. *et al.* Alzheimer's disease: Risk factors and potentially protective measures. *J. Biomed. Sci.* **26**, (2019).

30. Scarmeas, N., Stern, Y., Tang, M. X., Mayeux, R. & Luchsinger, J. A. Mediterranean diet and risk for Alzheimer's disease. *Ann. Neurol.* **59**, 912–921 (2006).

31. Santos, C. Y. *et al.* Pathophysiologic relationship between Alzheimer's disease, cerebrovascular disease, and cardiovascular risk: A review and synthesis. *Alzheimer's and Dementia: Diagnosis, Assessment and Disease Monitoring* **7**, 69–87 (2017).

32. Jack, C. R. *et al.* NIA-AA Research Framework: Toward a biological definition of Alzheimer's disease. *Alzheimers. Dement.* **14**, 535–562 (2018).

33. Koychev, I. *et al.* PET Tau and Amyloid-β Burden in Mild Alzheimer's Disease: Divergent Relationship with Age, Cognition, and Cerebrospinal Fluid Biomarkers. *J. Alzheimer's Dis.* **60**, 283–293 (2017).

34. Bakker, A., Albert, M. S., Krauss, G., Speck, C. L. & Gallagher, M. Response of the medial temporal lobe network in amnestic mild cognitive impairment to therapeutic intervention assessed by fMRI and memory task performance. *NeuroImage. Clin.* **7**, 688–98 (2015).

35. Crane, P. K. *et al.* Item response theory facilitated co-calibrating cognitive tests

and reduced bias in estimated rates of decline. *J. Clin. Epidemiol.* **61**, 1018 (2008).

36. Katz, L. C. & Shatz, C. J. Synaptic activity and the construction of cortical circuits. *Science* **274**, 1133–1138 (1996).

37. Selkoe, D. J. Alzheimer's disease is a synaptic failure. *Science* **298**, 789–791 (2002).

38. Rissman, R. A. & Mobley, W. C. Implications for treatment: GABAA receptors in aging, Down syndrome and Alzheimer's disease. *Journal of Neurochemistry* **117**, 613–622 (2011).

39. Luchetti, S., Huitinga, I. & Swaab, D. F. Neurosteroid and GABA-A receptor alterations in Alzheimer's disease, Parkinson's disease and multiple sclerosis. *Neuroscience* **191**, 6–21 (2011).

40. Alberdi, E. *et al. Amyloid β oligomers induce Ca 2+ dysregulation and neuronal death through activation of ionotropic glutamate receptors*. Cell calcium, 47, 3, (2010)

41. Sieghart, W. & Savić, M. M. International Union of Basic and Clinical Pharmacology. CVI: GABAA Receptor Subtype- and Function-selective Ligands: Key Issues in Translation to Humans. *Pharmacol. Rev.* **70**, 836–878 (2018).

42. Ulrich, D. Amyloid-β impairs synaptic inhibition via GABAA receptor endocytosis. *J. Neurosci.* **35**, 9205–9210 (2015).

43. Sahara, S., Yanagawa, Y., O'Leary, D. D. M. & Stevens, C. F. The fraction of cortical GABAergic neurons is constant from near the start of cortical neurogenesis to adulthood. *J. Neurosci.* **32**, 4755–61 (2012).

44. Sun, B. *et al.* Imbalance between GABAergic and Glutamatergic Transmission

Impairs Adult Neurogenesis in an Animal Model of Alzheimer's Disease. *Cell Stem Cell* **5**, 624–33 (2009).

45. Vogels, T. P., Sprekeler, H., Zenke, F., Clopath, C. & Gerstner, W. Inhibitory plasticity balances excitation and inhibition in sensory pathways and memory networks. *Science* **334**, 1569–73 (2011).

46. Zhou, S. & Yu, Y. Synaptic E-I Balance Underlies Efficient Neural Coding. *Front. Neurosci.* **12**, 46 (2018).

47. Gao, R. & Penzes, P. Common mechanisms of excitatory and inhibitory imbalance in schizophrenia and autism spectrum disorders. *Curr. Mol. Med.* **15**, 146–67 (2015).

48. Vico Varela, E., Etter, G. & Williams, S. Excitatory-inhibitory imbalance in Alzheimer's disease and therapeutic significance. *Neurobiology of Disease* **127**, 605–615 (2019).

49. Busche, M. A. & Konnerth, A. Impairments of neural circuit function in Alzheimer's disease. *Philos. Trans. R. Soc. Lond. B. Biol. Sci.* **371**, (2016).

50. Needs, H. I. *et al.* Changes in excitatory and inhibitory receptor expression and network activity during induction and establishment of epilepsy in the rat Reduced Intensity Status Epilepticus (RISE) model. *Neuropharmacology* **158**, 107728 (2019).

51. Minkeviciene, R. *et al.* Amyloid β-induced neuronal hyperexcitability triggers progressive epilepsy. *J. Neurosci.* **29**, 3453–3462 (2009).

52. Palop, J. J. *et al.* Aberrant Excitatory Neuronal Activity and Compensatory Remodeling of Inhibitory Hippocampal Circuits in Mouse Models of Alzheimer's

Disease. *Neuron* **55**, 697–711 (2007).

53. Holth, J. K. *et al.* Tau loss attenuates neuronal network hyperexcitability in mouse and Drosophila genetic models of epilepsy. *J. Neurosci.* **33**, 1651–9 (2013).

54. Demuro, A., Parker, I. & Stutzmann, G. E. Calcium Signaling and Amyloid Toxicity in Alzheimer Disease. (2010). doi:10.1074/jbc.R109.080895

55. Busche, M. A. *et al.* Clusters of Hyperactive Neurons Near Amyloid Plaques in a Mouse Model of Alzheimer's Disease. *Science (80-.).* **321**, 1686–1689 (2008).

56. Ramadan, J. W., Steiner, S. R., O'Neill, C. M. & Nunemaker, C. S. The central role of calcium in the effects of cytokines on beta-cell function: Implications for type 1 and type 2 diabetes. *Cell Calcium* **50**, 481–490 (2011).

57. Calcium Hypothesis Workgroup, A. Calcium Hypothesis of Alzheimer's disease and brain aging: A framework for integrating new evidence into a comprehensive theory of pathogenesis. Alzheimer's & dementia : the journal of the Alzheimer's Association, **13**, 2, 2 (2017)

58. Bateman, R. J. *et al.* Clinical and biomarker changes in dominantly inherited Alzheimer's disease. *N. Engl. J. Med.* **367**, 795–804 (2012).

59. Vlassenko, A. G., Benzinger, T. L. S. & Morris, J. C. PET amyloid-beta imaging in preclinical Alzheimer's disease. *Biochim. Biophys. Acta* **1822**, 370–9 (2012).

60. Quiroz, Y. T. *et al.* Hippocampal hyperactivation in presymptomatic familial Alzheimer's disease. *Ann. Neurol.* **68**, 865–875 (2010).

61. Bookheimer, S. Y. *et al.* Patterns of Brain Activation in People at Risk for Alzheimer's Disease. *N. Engl. J. Med.* **343**, 450–456 (2000).

62. Putcha, D. *et al.* Hippocampal hyperactivation associated with cortical thinning in

Alzheimer's disease signature regions in non-demented elderly adults. *J. Neurosci.* **31**, 17680–8 (2011).

63. Bakker, A. *et al.* Reduction of hippocampal hyperactivity improves cognition in amnestic mild cognitive impairment. *Neuron* **74**, 467–74 (2012).

64. Pandis, D. & Scarmeas, N. Seizures in Alzheimer disease: clinical and epidemiological data. *Epilepsy Curr.* **12**, 184–7 (2012).

65. Pasquini, L. *et al.* Medial Temporal Lobe Disconnection and Hyperexcitability Across Alzheimer's Disease Stages. *J. Alzheimer's Dis. reports* **3**, 103–112 (2019).

66. Pasquini, L. *et al.* Increased Intrinsic Activity of Medial-Temporal Lobe Subregions is Associated with Decreased Cortical Thickness of Medial-Parietal Areas in Patients with Alzheimer's Disease Dementia. *J. Alzheimer's Dis.* **51**, 313–326 (2016).

67. Raichle, M. E. *et al.* A default mode of brain function. *Proc. Natl. Acad. Sci. U. S. A.* **98**, 676–682 (2001).

68. Sperling, R. A. *et al.* Amyloid deposition is associated with impaired default network function in older persons without dementia. *Neuron* **63**, 178–88 (2009).

69. Mevel, K., Chételat, G., Eustache, F. & Desgranges, B. The default mode network in healthy aging and Alzheimer's disease. *Int. J. Alzheimers. Dis.* **2011**, 535816 (2011).

70. Hagmann, P. *et al.* Mapping the structural core of human cerebral cortex. *PLoS Biol.* **6**, e159 (2008).

71. Raichle, M. E. The Brain's Default Mode Network. *Annu. Rev. Neurosci.* **38**, 433–

447 (2015).

72. Harrison, B. J. *et al.* Task-Induced Deactivation from Rest Extends beyond the Default Mode Brain Network. *PLoS One* **6**, e22964 (2011).

73. Mayer, J. S., Roebroeck, A., Maurer, K. & Linden, D. E. J. Specialization in the default mode: Task-induced brain deactivations dissociate between visual working memory and attention. *Hum. Brain Mapp.* **31**, NA-NA (2009).

74. Singh, K. D. & Fawcett, I. P. Transient and linearly graded deactivation of the human default-mode network by a visual detection task. *Neuroimage* **41**, 100–112 (2008).

75. Palmqvist, S. *et al.* Earliest accumulation of β-amyloid occurs within the default-mode network and concurrently affects brain connectivity. *Nat. Commun.* **8**, 1214 (2017).

76. Buckner, R. L., Andrews-Hanna, J. R. & Schacter, D. L. The Brain's Default Network Anatomy, Function, and Relevance to Disease. *Am. Psychol. Assoc.* (2008). doi:10.1196/annals.1440.011

77. Verret, L. *et al.* Inhibitory Interneuron Deficit Links Altered Network Activity and Cognitive Dysfunction in Alzheimer Model. *Cell* **149**, 708–721 (2012).

78. Goutagny, R. & Krantic, S. Hippocampal oscillatory activity in Alzheimer's disease: toward the identification of early biomarkers? *Aging Dis.* **4**, 134–40 (2013).

79. Noebels, J. A perfect storm: Converging paths of epilepsy and Alzheimer's dementia intersect in the hippocampal formation. *Epilepsia* **52**, 39–46 (2011).

80. Styr, B. & Slutsky, I. Imbalance between firing homeostasis and synaptic plasticity

drives early-phase Alzheimer's disease. *Nat. Neurosci.* **21**, 463–473 (2018).

81. Okun, M. & Lampl, I. Instantaneous correlation of excitation and inhibition during ongoing and sensory-evoked activities. *Nat. Neurosci.* **11**, 535–537 (2008).

82. Barral, J. & D'Reyes, A. Synaptic scaling rule preserves excitatory-inhibitory balance and salient neuronal network dynamics. *Nat. Neurosci.* **19**, 1690–1696 (2016).

83. Limon, A., Reyes-Ruiz, J. M. & Miledi, R. Loss of functional GABAA receptors in the Alzheimer diseased brain. *Proc. Natl. Acad. Sci.* **109**, 10071–10076 (2012).

84. Jayadev, S. *et al.* Alzheimer's disease phenotypes and genotypes associated with mutations in presenilin 2. *Brain* **133**, 1143–1154 (2010).

85. L, C. *et al.* Phenotype associated with APP duplication in five families. *Brain* **129**, 2966–2976 (2006).

86. Palop, J. J. & Mucke, L. Epilepsy and cognitive impairments in Alzheimer disease. *Arch. Neurol.* **66**, 435–40 (2009).

87. HE, S. 'Untangling' Alzheimer's disease and epilepsy. *Epilepsy Curr.* **12**, 178–183 (2012).

88. Xue, M., Atallah, B. V & Scanziani, M. Equalizing excitation-inhibition ratios across visual cortical neurons. *Nature* **511**, 596–600 (2014).

89. T, K. & P, S. Neuronal diversity and temporal dynamics: the unity of hippocampal circuit operations. *Science* **321**, 53–57 (2008).

90. P, F. *et al.* Synaptic and extrasynaptic origin of the excitation/inhibition imbalance in the hippocampus of synapsin I/II/III knockout mice. *Cereb. Cortex* **23**, 581–593 (2013).

91. Barron, H. C., Vogels, T. P., Behrens, T. E., Ramaswami, M. Inhibitory engrams in perception and memory. Proceedings of the National Academy of Sciences, **114**, 26, 6 (2017)

92. Mariño, J. *et al.* Invariant computations in local cortical networks with balanced excitation and inhibition. *Nat. Neurosci.* **8**, 194–201 (2005).

93. Vogels, T. P. & Abbott, L. F. Gating multiple signals through detailed balance of excitation and inhibition in spiking networks. *Nat. Neurosci.* **12**, 483–491 (2009).

94. Yamada, K. *et al.* Neuronal activity regulates extracellular tau in vivo. *J. Exp. Med.* **211**, 387–393 (2014).

95. Cirrito, J. R. *et al.* Synaptic Activity Regulates Interstitial Fluid Amyloid-β Levels In Vivo. *Neuron* **48**, 913–922 (2005).

96. Uddin, L. Q., Kelly, A. M. C., Biswal, B. B., Castellanos, F. X. & Milham, M. P. Functional Connectivity of Default Mode Network Components: Correlation, Anticorrelation, and Causality. *Hum. Brain Mapp.* **30**, 625–637 (2009).

97. Zott, B., Busche, M. A., Sperling, R. A. & Konnerth, A. What Happens with the Circuit in Alzheimer's Disease in Mice and Humans? *Annu. Rev. Neurosci.* **41**, 277–297 (2018).

98. Lustig, C. *et al.* Functional deactivations: Change with age and dementia of the Alzheimer type. *Proc. Natl. Acad. Sci. U. S. A.* **100**, 14504–14509 (2003).

99. Head, E., Powell, D., Gold, B. T. & Schmitt, F. A. *Alzheimer's Disease in Down Syndrome*.

100. Limon, A., Reyes-Ruiz, J. M. & Miledi, R. Microtransplantation of neurotransmitter receptors from postmortem autistic brains to Xenopus oocytes.

Proc. Natl. Acad. Sci. U. S. A. **105**, 10973–10977 (2008).

101. Eusebi, F., Palma, E., Amici, M. & Miledi, R. Microtransplantation of ligand-gated receptor-channels from fresh or frozen nervous tissue into Xenopus oocytes: A potent tool for expanding functional information. *Progress in Neurobiology* **88**, 32–40 (2009).

102. Zwart, R., Mazzo, F. & Sher, E. Microtransplantation of human brain receptors into oocytes to tackle key questions in drug discovery. *Drug Discovery Today* **24**, 533–543 (2019).

103. Mazzo, F. *et al.* Reconstitution of synaptic Ion channels from rodent and human brain in *Xenopus* oocytes: a biochemical and electrophysiological characterization. *J. Neurochem.* **138**, 384–396 (2016).

104. Bernareggi, A. *et al.* Characterization of GABAA receptors expressed in glial cell membranes of adult mouse neocortex using a Xenopus oocyte microtransplantation expression system. *J. Neurosci. Methods* **198**, 77–83 (2011).

105. Agarwal, S., Tannenberg, R. K. & Dodd, P. R. Reduced expression of the inhibitory synapse scaffolding protein gephyrin in Alzheimer's disease. *J. Alzheimers. Dis.* **14**, 313–21 (2008).

106. Scaduto, P., Sequeira, A., Vawter, M. P., Bunney, W. & Limon, A. Preservation of global synaptic excitatory to inhibitory ratio during long postmortem intervals. *Sci. Rep.* **10**, 1–8 (2020).

107. Hales, C. M. *et al.* Abnormal Gephyrin immunoreactivity associated with Alzheimer disease pathologic changes. *J. Neuropathol. Exp. Neurol.* **72**, 1009–1015 (2013).

108. Mondragón-Rodríguez, S. *et al.* Interaction of endogenous tau protein with synaptic proteins is regulated by N-methyl-D-aspartate receptor-dependent tau phosphorylation. *J. Biol. Chem.* **287**, 32040–32053 (2012).

109. Ittner, A. & Ittner, L. M. Dendritic Tau in Alzheimer's Disease. *Neuron* **99**, 13–27 (2018).

110. Froemke, R. C. Plasticity of Cortical Excitatory-Inhibitory Balance. *Annu. Rev. Neurosci.* **38**, 195–219 (2015).

111. Turrigiano, G. G., Leslie, K. R., Desai, N. S., Rutherford, L. C. & Nelson, S. B. Activity-dependent scaling of quantal amplitude in neocortical neurons. *Nature* **391**, 892–896 (1998).

112. Turrigiano, G. Homeostatic synaptic plasticity: local and global mechanisms for stabilizing neuronal function. *Cold Spring Harb. Perspect. Biol.* **4**, a005736 (2012).

113. Greicius, M. D., Srivastava, G., Reiss, A. L. & Menon, V. Default-mode network activity distinguishes Alzheimer's disease from healthy aging: evidence from functional MRI. *Proc. Natl. Acad. Sci. U. S. A.* **101**, 4637–42 (2004).

114. Lee, E. S. *et al.* Default Mode Network Functional Connectivity in Early and Late Mild Cognitive Impairment: Results from the Alzheimer's Disease Neuroimaging Initiative. *Alzheimer Dis. Assoc. Disord.* **30**, 289–296 (2016).

115. Bjorklund, N. L. *et al.* Absence of amyloid β oligomers at the postsynapse and regulated synaptic Zn2+in cognitively intact aged individuals with Alzheimer's disease neuropathology. *Mol. Neurodegener.* **7**, (2012).

116. Zolochevska, O. & Taglialatela, G. Non-Demented Individuals with Alzheimer's

Disease Neuropathology: Resistance to Cognitive Decline May Reveal New Treatment Strategies. *Curr. Pharm. Des.* **22**, 4063–8 (2016).

117. Vega, J. N., Hohman, T. J., Pryweller, J. R., Dykens, E. M. & Thornton-Wells, T. A. Resting-state functional connectivity in individuals with down syndrome and williams syndrome compared with typically developing controls. *Brain Connect.* **5**, 461–475 (2015).

118. Miller, J. A. *et al.* Neuropathological and transcriptomic characteristics of the aged brain. *Elife* **6**, (2017).

119. Bookheimer, S. Y. *et al.* Patterns of Brain Activation in People at Risk for Alzheimer's Disease. *N. Engl. J. Med.* **343**, 450–456 (2000).

120. Serra-Batiste, M. *et al.* Aβ42 assembles into specific β-barrel pore-forming oligomers in membrane-mimicking environments. *Proc. Natl. Acad. Sci.* **113**, 10866–10871 (2016).

121. Bode, D. C., Baker, M. D. & Viles, J. H. Ion Channel Formation by Amyloid-β42 Oligomers but Not Amyloid-β40 in Cellular Membranes. *J. Biol. Chem.* **292**, 1404 (2017).

122. ST, Creavin, S, Wisniewski, AH, Noel-Storr, CM, Trevelyan, T, Hampton, D, Rayment, VM, Thom, KJ, Nash, H, Elhamoui, R, Milligan, AS, Patel, DV, Tsivos, T, Wing, E, Phillips, SM, Kellman, HL, Shackleton, GF, Singleton, BE, Neale, ME, Watton, S, Cullum*et al.* Mini-Mental State Examination (MMSE) for the detection of dementia in clinically unevaluated people aged 65 and over in community and primary care populations. *Cochrane database Syst. Rev.* **2016**, (2016).

123. K, Shen., T, Zeppillo. & A, Limon. Regional transcriptome analysis of AMPA and GABA A receptor subunit expression generates E/I signatures of the human brain. *Sci. Rep.* **10**, (2020).

124. Sequeira, A., Shen, K., Gottlieb, A. & Limon, A. Human brain transcriptome analysis finds region- and subject-specific expression signatures of GABA A R subunits. *Commun. Biol. 2019 21* **2**, 1–14 (2019).

125. T, Zeppillo T, Zeppillo,A Schulmann, F, Macciardi, BE, Hjelm, M, Föcking, PA, Sequeira, I, Guella, D, Cotter, WE, Bunney, A, Limon, MP, Vawter. Functional impairment of cortical AMPA receptors in schizophrenia. *Schizophr. Res.* (2020). doi:10.1016/J.SCHRES.2020.03.037

126. Shen, K. & Limon, A. Transcriptomic expression of AMPA receptor subunits and their auxiliary proteins in the human brain. *Neurosci. Lett.* **755**, 135938 (2021).

127. Uezu, A. *et al.* Identification of an elaborate complex mediating postsynaptic inhibition. *Science (80-.).* **353**, 1123–1129 (2016).

128. Overview :: Allen Brain Atlas: Aging, Dementia and TBI Study. Available at: https://aging.brain-map.org/. (Accessed: 2nd August 2021)

129. Lauterborn, J. C. *et al.* Increased excitatory to inhibitory synaptic ratio in parietal cortex samples from individuals with Alzheimer's disease. *Nat. Commun.* **12**, (2021).

130. Braak, H. & Braak, E. Staging of alzheimer's disease-related neurofibrillary changes. *Neurobiol. Aging* **16**, 271–278 (1995).

131. Dick, M. B., Doran, E., Phelan, M. & Lott, I. T. Cognitive profiles on the severe Impairment Battery are similar in Alzheimer disease and Down syndrome with

dementia. *Alzheimer Dis. Assoc. Disord.* **30**, 251–257 (2016).

132. Lauterborn, J. C. *et al.* Synaptic actin stabilization protein loss in Down syndrome and Alzheimer disease. *Brain Pathol.* (2019). doi:10.1111/bpa.12779

133. Chen, L. Y., Rex, C. S., Casale, M. S., Gall, C. M. & Lynch, G. Changes in synaptic morphology accompany actin signaling during LTP. *J. Neurosci.* **27**, 5363–5372 (2007).

134. Hunt, C. A., Schenker, L. J. & Kennedy, M. B. PSD-95 is associated with the postsynaptic density and not with the presynaptic membrane at forebrain synapses. *J. Neurosci.* **16**, 1380–1388 (1996).

135. Rex, C. S. *et al.* Different Rho GTPase-dependent signaling pathways initiate sequential steps in the consolidation of long-term potentiation. *J. Cell Biol.* **186**, 85–97 (2009).

136. Chen, L. Y. *et al.* Physiological activation of synaptic Rac>PAK (p-21 activated kinase) signaling is defective in a mouse model of fragile X syndrome. *J. Neurosci.* **30**, 10977–10984 (2010).

137. Seese, R. R. *et al.* LTP induction translocates cortactin at distant synapses in wild-type but not Fmr1 knock-out mice. *J. Neurosci.* **32**, 7403–7413 (2012).

138. Gylys, K. H., Fein, J. A., Yang, F. & Cole, G. M. Enrichment of presynaptic and postsynaptic markers by size-based gating analysis of synaptosome preparations from rat and human cortex. *Cytometry* **60A**, 90–96 (2004).

139. Comerota, M. M., Krishnan, B. & Taglialatela, G. Near infrared light decreases synaptic vulnerability to amyloid beta oligomers. *Sci. Rep.* **7**, (2017).

140. Gylys, K. H. *et al.* Synaptic changes in alzheimer's disease: Increased amyloid-β

and gliosis in surviving terminals is accompanied by decreased PSD-95 fluorescence. *Am. J. Pathol.* **165**, 1809–1817 (2004).

141. Marsal, J., Tigyi, G. & Miledi, R. Incorporation of acetylcholine receptors and Cl-channels in Xenopus oocytes injected with Torpedo electroplaque membranes. *Proc. Natl. Acad. Sci. U. S. A.* **92**, 5224–8 (1995).

142. Maestú, F., de Haan, W., Busche, M. A. & DeFelipe, J. Neuronal excitation/inhibition imbalance: core element of a translational perspective on Alzheimer pathophysiology. *Ageing Res. Rev.* **69**, 101372 (2021).

143. Yamada, K. *et al.* Neuronal activity regulates extracellular tau in vivo. *J. Exp. Med.* **211**, 387–93 (2014).

144. Pooler, A. M., Phillips, E. C., Lau, D. H. W., Noble, W. & Hanger, D. P. Physiological release of endogenous tau is stimulated by neuronal activity. *EMBO Rep.* **14**, 389–394 (2013).

145. Maxim Iascone, D. *et al.* Whole-Neuron Synaptic Mapping Reveals Spatially Precise Excitatory/Inhibitory Balance Limiting Dendritic and Somatic Spiking. *Neuron* **106**, 566-578.e8 (2020).

146. Amatniek, J. C. *et al.* Incidence and Predictors of Seizures in Patients with Alzheimer's Disease. *Epilepsia* **47**, 867–872 (2006).

147. Cortini, F., Cantoni, C. & Villa, C. Epileptic seizures in autosomal dominant forms of Alzheimer's disease. *Seizure - Eur. J. Epilepsy* **61**, 4–7 (2018).

148. J, DeFelipe, L, Alonso-Nanclares, JI, Arellano. Microstructure of the neocortex: comparative aspects. *J. Neurocytol.* **31**, 299–316 (2002).

149. SH, Zaman, A, Parent, A, Laskey, MK, Lee, DR, Borchelt, SS, Sisodia, R,

Malinow. Enhanced synaptic potentiation in transgenic mice expressing presenilin 1 familial Alzheimer's disease mutation is normalized with a benzodiazepine. *Neurobiol. Dis.* **7**, 54–63 (2000).

150. Palop, Jorge J., Mucke, Lennart. Network abnormalities and interneuron dysfunction in Alzheimer disease. *Nat. Rev. Neurosci.* **17**, 777–792 (2016).

151. M, Mikkonen, I, Alafuzoff, T, Tapiola, H, Soininen, R, Miettinen. Subfield- and layer-specific changes in parvalbumin, calretinin and calbindin-D28K immunoreactivity in the entorhinal cortex in Alzheimer's disease. *Neuroscience* **92**, 515–532 (1999).

152. V, Garcia-Marin, L, Blazquez-Llorca, JR, Rodriguez, S, Boluda, G, Muntane I, Ferrer, J, Defelipe. Diminished perisomatic GABAergic terminals on cortical neurons adjacent to amyloid plaques. *Front. Neuroanat.* **3**, (2009).

153. Kandimalla, R. & Reddy, P. H. Therapeutics of Neurotransmitters in Alzheimer's Disease. *J. Alzheimers. Dis.* **57**, 1049–1069 (2017).

154. Y, Xu, J, Yan, P, Zhou, J, Li, H, Gao, Y, Xia, Q, Wang. Neurotransmitter receptors and cognitive dysfunction in Alzheimer's disease and Parkinson's disease. *Prog. Neurobiol.* **97**, 1–13 (2012).

155. Govindpani, Karan, Guzmán, Beatriz Calvo-Flores, Vinnakota, Chitra, Waldvogel, Henry J., Faull, Richard L., Kwakowsky, Andrea. Towards a Better Understanding of GABAergic Remodeling in Alzheimer's Disease. *Int. J. Mol. Sci.* **18**, (2017).

VITA

Pietro Scaduto was born in Palermo in 1990.

Awards:

Aug.2021	**2021 Alzheimer Award - Winning paper** The Journal of Alzheimer's Disease (JAD)
Dic.2020	**Dennis William Bowman Scholarship in Biomedical Research** University Texas Medical Branch, TX, U.S.A
Nov.2020	**Outstanding Leadership Award - 5th Annual NGP Student Symposium** University Texas Medical Branch, TX, U.S.A
Nov.2020	**First place winner for Session II, Day 1 of the 5th Annual NGP Student Symposium** University Texas Medical Branch, TX, U.S.A
Aug.2020	**Graduate School of Biomedical Sciences 50/50 Endowment Scholarship Award** University Texas Medical Branch, TX, U.S.A
Jan.2020	**Rose and Harry Walk Memorial Award** University Texas Medical Branch, TX, U.S.A
Jan.2019	**Mason Guest Scholar Program Award** University Texas Medical Branch, TX, U.S.A
Jul. 2016	**Board exam and licensed to practice as a Biologist in Italy.** The University of Palermo, Italy.
Aug.2012	**Travel Grant award "viaggi e soggiorni di studio per gli studenti"** organized by the University of Palermo. From Sept.2012 until Dic.2012, he attended the laboratory of Neurophysiology, directed by Prof. Giuseppe Di Giovanni, at the Department of Physiology and biochemistry of the University of Malta.
Sept. 2010	**Erasmus scholarship award** for a study period of nine months at the Universidad Complutense de Madrid, Spain

Publications:

Scaduto P, Sequeira A, Vawter M, Bunney W, Limon A. Preservation of global synaptic E/I ratio during long postmortem Intervals. Scientific Report. 2020 May 25;10(1):8626. doi: 10.1038/s41598-020-65377-3.

Frinchi M*, **Scaduto P***, Cappello F, Belluardo N, Mudò G. Heat shock protein (Hsp) regulation by muscarinic acetylcholine receptor (mAChR) activation in the rat hippocampus. J Cell Physiol. 2018 Aug;233(8):6107-6116. doi: 10.1002/jcp.26454. Epub 2018 Mar 6. **[*co-first author].**

Singh A, Allen D, Fracassi A, Tumurbaatar B, Natarajan C, **Scaduto P**, Woltjer R, Kayed R, Limon A, Krishnan B and Taglialatela G. Functional integrity of synapses in the central nervous system of cognitively intact individuals with high Alzheimer's neuropathology is associated with absence of synaptic tau oligomers. J Alzheimers Dis. 2020 Oct ;78(4):1661-1678. doi: 10.3233/JAD-200716.

Mudò G, Frinchi M, Nuzzo D, **Scaduto P**, Plescia F, Massenti MF, Di Carlo M, Cannizzaro C, Cassata G, Cicero L, Ruscica M, Belluardo N, Grimaldi LM. Anti-inflammatory and cognitive effects of Interferon-β1a (IFNβ1a) in a rat model of Alzheimer's disease". J Neuroinflammation. 2019 Feb 18;16(1):44. doi: 10.1186/s12974-019-1417-4.

Liu Z, Wadsworth P, Singh AK, Chen H, Wang P, Folorunso O, **Scaduto P**, Ali SR, Laezza F, Zhou J. Identification of peptidomimetics as novel chemical probes modulating fibroblast growth factor 14 (FGF14) and voltage-gated sodium channel 1.6 (Nav1.6) protein-protein interactions. Bioorg Med Chem Lett. 2019 Feb 1;29(3):413-419. doi: 10.1016/j.bmcl.2018.12.031. Epub 2018 Dec 15.

Frinchi M, Nuzzo D, **Scaduto P** , Di Carlo M, Massenti MF , Belluardo N, Mudò G. Anti-inflammatory and antioxidant effects of muscarinic acetylcholine receptor (mAChR) activation in the rat hippocampus. Sci Rep. 2019 Oct 2;9(1):14233. doi: 10.1038/s41598-019-50708-w.

Lauterborn JC, **Scaduto P**, Lynch G, Gall CM, Keene CD, Jennings K, Limon A. Increased Functional Excitatory/Inhibitory Synaptic Ratio in Parietal Cortex of Alzheimer's Disease but not Down Syndrome. Nat Commun. 2021 May 10;12(1):2603.doi: 10.1038/s41467-021-22742-8.

Permanent address: Via A. Catalano, 6. Bagheria (PA), 90011, Italy

U.S address: 9600 Golf Lakes Trail, Dallas, TX 75231

This dissertation was typed by Pietro Scaduto